CIRCADIAN FLUX OF EXTRAVASCULAR POLYMORPHONUCLEAR LEUKOCYTES IN THE MOUSE LIMBUS

By

Vanna Pham
O.D. University of Houston, 2019
B. Sc. University of Houston, 2014

THESIS

In partial satisfaction of the requirements for the degree of

MASTERS OF SCIENCE

In

PHYSIOLOGICAL OPTICS AND VISION SCIENCE

Presented to the Graduate Faculty of the

College of Optometry
University of Houston
Department of Physiological Optics and Vision Sciences

May 2019

Approved:

Alan R. Burns, Ph.D. (Chair)

C. Wayne Smith, M.D.

Samuel Hanlon, O.D., Ph.D.

Dedication

To my mom, dad, Phammers, and Daniel. You all were my backbone and support throughout this entire journey.

Acknowledgments

I would like to express a tremendous thank you to Dr. Burns for being the greatest mentor. You were always encouraging with your humor and enthusiasm. Thank you for all of your kindness and patience as well as imparting endless knowledge on this project. Had it not been for your convincing and inspiring comments during our conversations, starting from the tour of the lab to my decision whether to continue with the Masters, I would not have made it this far.

I would like to thank my committee members, Dr. Hanlon and Dr. Smith for their valuable time and support. I truly appreciate all of your wisdom and insight, which made it possible for the completion of this thesis.

I would like to send warm gratitude to Dr. Frishman, the chair of UHCO's graduate program, whose encouragement, flexibility, and understanding helped me navigate the complexities of this combined OD/MS program. My sincere thanks also goes to Renee Acosta, who played an enormous role in the graduate program as well.

To Aubrey, Sri, Justin, Eugene, Angie, and Paul, thank you for all of your mentorship and camaraderie during our journey in the lab together. My thanks and appreciation also goes to Pooja and Apoorva for their time and contribution to the project.

I would also like to thank everyone at UHCO, from my Class of 2019 colleagues to my amazing attendings and professors, for their ongoing support.

A special word of gratitude is due to all of my dearest friends and family, especially Daniel Lorenzana, for your encouragement, patience, and motivation to help keep me going all these years. Thanks to everyone for believing in me.

Circadian Flux of Extravascular Polymorphonuclear Leukocytes in the Mouse Limbus

By

Vanna Pham, O.D.

May 2019

Abstract

Purpose: In the uninjured mouse cornea, a recent study suggests extravascular PMNs are found at the limbus and their numbers rise and fall in a circadian rhythm, peaking in the evening. Additional studies in other tissues suggest metabolic syndrome resulting from the consumption of a HFD is associated with circadian disturbances. The studies outlined in this thesis were designed to test the **hypothesis** that the circadian accumulation of PMNs at the limbus is depressed by consumption of a HFD. **Aim 1** will determine if there is a circadian flux of PMN extravasation at the limbus in the uninjured cornea, and **Aim 2** will determine if consumption of a HFD affects PMN extravasation at the limbus.

Methods: C57BL/6 male mice (7 weeks of age; n=65 total) were fed a normal diet (ND) or a HFD. Some mice were euthanized at 3h time intervals spanning a 24h period while other mice were euthanized at one of two time-points, evening (9 pm or 11 pm) or morning (11 am or 12 pm). Excised corneas were immunostained for PMNs and blood vessels. Using a DeltaVision fluorescence microscope, the limbal area for each cornea was measured and the total number of extravascular limbal PMNs was determined. Data are shown as mean ± SD and statistical significance was set at $p \leq 0.05$.

Results: PMN infiltration at the limbus followed a circadian pattern and PMN numbers were ~30% higher in the evening ($p \leq 0.05$), but only after pooling the data to increase the sample size (n=20). Pooling was not possible for the HFD studies (n=5) and PMN counts were not significantly difference between mice fed a ND or a HFD.

Conclusion: Collectively, the data show a large sample size is needed to evaluate PMN accumulation at the limbus. PMNs show a significant peak accumulation in the evening, but statistical significance is only evident after pooling the data to increase sample size (n=20). Pooling was not possible for the HFD study and no firm conclusions can be drawn because the study was underpowered by virtue of its smaller sample size (n=5).

Table of Contents

Dedication iv
Acknowledgments v
Abstract vii
List of Abbreviations x
List of Figures 1
List of Tables 2
Chapter One: Introduction 3
Preface 4
Introduction: Anatomy and Physiology Review of the Human Cornea 5
Human Limbus 9
The Mouse Cornea and Limbus as an Experimental Model 11
Polymorphonuclear leukocytes 14
Circadian Rhythm 18
Metabolic syndrome 20
Summary and Objectives 24
Chapter 2: Materials and Methods 26
2.1 Sources of Materials 26
Animals 26
Diet composition and feeding schedule 26
Tissue Processing 27
Immunolabeling and preparation of slides 28
Fluorescence Imaging 30
Specific Methods for Enumeration of PMNs 30
PMN Enumeration 30
Electrocautery 33
Adjustment for Radial Cuts 34
Statistical Analysis 38
Experiment 1 38
Experiment 2 39
Experiment 3 39
Experiment 4 39
Pooling of data 39

Chapter 3: Results....40
Overview of Data Collection....41
Experiment 1: Extravascular PMN counts showed a peak and nadir over a 24-hour period....41
Interobserver Data Analysis....46
PMN extravasation across four quadrants was not similar....47
Experiments 2-4....51
Experiment 2: PMN counts were similar in morning and evening after increase in sample size....51
Experiment 3: PMN counts were similar in morning and evening after increase in sample size....52
Experiment 4: Feeding mice a HFD for 10 days did not affect PMN extravasation....52
Pooling data from experiments 1-4 revealed a circadian pattern to PMN extravasation at the limbus....55
Chapter 4: Discussion....56
Aims for this thesis:....57
HFD feeding revealed non-confirmative conclusions on PMN circadian flux....57
The need for a larger sample size when analyzing PMN circadian flux....58
Our results showed a modest increase in PMN counts....58
Significance of this study....59
Why are PMNs present in uninjured limbus?....59
PMN extravasation at the limbus is not uniform in all quadrants....61
Influx of PMNs during non-inflammatory conditions....62
Clinical Implications....69
The clinical relevance of studying circadian rhythm in the mouse model....69
Why do we study circadian rhythm?....69
General Conclusions and Future Directions....72
Strengths in our study....72
Limitations of this study and ways to improve future studies:....73
Future Directions....74
Bibliography (or References)....76

List of Abbreviations

µg	Micrograms
µm	Micrometers; microns
ad lib	*ad libitum*
ALL	Anterior limiting lamina
ANOVA	Analysis of variance
APC	Allophycocyanin
ARVO	Association for Research and Vision in Ophthalmology
BSA	Bovine serum albumin
Cy-5	Cyanine dye 5
DAPI	4', 6-diamidino-2-phenylindole
DIO	Diet-induced obesity
FITC	Fluorescein isothiocyanate
HFD	High fat diet
HRT-RCM	Heidelberg Retinal Tomographer III/ Rostock Corneal Module
ICAM-1	Intracellular cell adhesion molecule-1
IL-17	Interleukin 17
Kcal	Kilocalories
MetS	Metabolic syndrome
mm	Millimeter
ND	Normal diet
PBS	Phosphate buffered saline
PLL	Posterior limiting lamina
PMN	Polymorphonuclear leukocyte; neutrophil

RT	Room temperature
SD	Standard deviation
SEM	Standard error of the mean
TRITC	Tetramethylrhodamine
VEGF	Vascular endothelial growth factor
ZT	Zeitgeber time

List of Figures

Figure 1. Illustration of the human corneal layers: epithelium, anterior limiting lamina, stroma, posterior limiting lamina, and endothelium 6
Figure 2: Extravascular polymorphonuclear leukocyte 16
Figure 3. Corneal nerve changes may result from diet-induced obesity 21
Figure 4. HFD suppresses corneal expression of Rev-erb alpha 22
Figure 5. Extravascular PMNs in the nasal region of the limbus at 12 AM 31
Figure 6. Utilizing two excitation/emission channels to view vasculature and PMNs 32
Figure 7. Limbus in the flat-mounted cornea from the left eye 33
Figure 8. Two examples of electrocautery to label superior quadrant, showing equal radial cuts and unequal radial cuts 35
Figure 9. Schema demonstrating flat mounted corneas with radial cuts that result in a centered or off-centered electrocautery mark 36
Figure 10. Schema showing flat mounted corneas with redistribution of the quadrants 37
Figure 11. Extravascular PMN counts at the limbus in the uninjured mouse cornea during a 24h period. 42
Figure 12. PMN extravasation at 12 PM and 9 PM in the superior quadrant of the mouse limbus. 43
Figure 13: Extravasated PMNs by limbal regions at 8 time intervals 45
Figure 14. Interobserver data comparison for experiment 1 46
Figure 15. Extravasting PMNs for anatomical regions in the mouse limbus 50
Figure 16. There was no apparent difference in PMN counts between 11 PM and 11 AM or between HFD and ND counts in 20 corneas 54
Figure 17. PMN extravasation appears to favor capillary loops region at both 12 PM and 9 PM 64
Figure 18. PMN extravasation in the limbus during inflammation and (proposed mechanism) during non-inflammation 66

List of Tables

Table 1. Summary of Human vs. Mouse Anatomy 13
Table 2. Fluorescent Markers 29
Table 3. PMN Counts/quadrant across 8 time-intervals (n=3) in 24h period 48
Table 4. Chi Square Test Results 49
Table 5. Metabolic syndrome parameters in mice fed a ND or HFD for 10 days 53

Chapter One: Introduction

PREFACE
1.1 Introduction: Anatomy and Physiology Review of the Human Cornea
1.2 Human Limbus
    1.2.1 The Limbus and its Function
    1.2.2 Defining the Limbal Regions
    1.2.3 Limbal Vasculature and its Role
1.3 The Mouse Cornea and Limbus as an Experimental Model
1.4 Neutrophils
    1.4.1 Role of a Neutrophil
    1.4.2 Neutrophil Accumulation in Inflammation and Non-inflammation
1.5 Circadian Rhythm
1.5.1 Circadian Rhythms in mammals
1.5.2 Homing of PMNs within tissues in a circadian pattern
1.6 Metabolic Syndrome
1.7 Effect of Metabolic Syndrome on Circadian Rhythm
1.8 Summary and Objectives

Preface

This thesis evaluates the effect of a high fat diet (HFD) and the resulting metabolic syndrome on neutrophil (PMN) uninjured extravasation from the mouse corneal limbal vasculature. PMN extravasation at the limbus is a normal activity that occurs in the unperturbed cornea, not requiring injury or infection. A recent publication proposes PMN extravasation may follow a circadian rhythm, peaking in the evening. The purpose served by extravasation is unclear, but it may relate to homeostatic maintenance of corneal nerves. This concept is supported by three observations. First, VEGF secretion by infiltrating PMNs speeds nerve recovery in the injured cornea. Second, our unpublished data demonstrate that uninjured corneas from mice fed a HFD exhibit a significant loss in nerve sensation. Third, several studies in the literature show metabolic syndrome resulting from the consumption of a HFD is associated with circadian disturbances. The **purpose of this thesis** to determine in the mouse 1) if there is a circadian flux of PMN extravasation at the limbus in an uninjured mouse cornea, and 2) if PMN extravasation at the limbus is affected by consumption of a HFD.

The following introduction provides the rationale behind our **working hypothesis** that in the mouse, PMN limbal uninjured extravasation follows a circadian rhythm and this rhythm is blunted by feeding the mice a HFD. This introduction begins with an anatomical review of the cornea and limbal vasculature. This is preceded by a review of the life cycle and behavior of PMNs under non-inflammatory and inflammatory conditions. Evidence for a circadian pattern of infiltration in the cornea and other non-inflamed tissues is considered as a role for PMNs in corneal nerve regeneration. Finally, evidence supporting the necessity of PMN extravasation for corneal nerve regeneration

will be discussed in addition to the influence of metabolic syndrome on corneal homeostasis.

Introduction: Anatomy and Physiology Review of the Human Cornea

The cornea is a transparent, avascular tissue that is essential for clear vision. The human cornea measures approximately 11.5 mm horizontally and 10.5 mm vertically, and the central anterior radius of curvature is 7.8 mm[1]. When combined with the overlying tear film to form the tear-film interface, the cornea provides approximately two-thirds of the refractive power of the eye. The outermost surface of the cornea is coated with a 3 µm thick tear film, which offers nutrients and protection in addition to refractive power. The cornea must remain clear to provide optimal vision, and its clarity stems from the organization of the tissue. The corneal tear film is separated into three sections: an aqueous layer in between two hydrophobic layers[2]. Traditionally, the human cornea is considered to have five layers, all contributing to homeostatic function. From anterior to posterior, the corneal layers are: epithelium, anterior limiting lamina (Bowman's layer), stroma, posterior limiting lamina (Descemet's membrane), and endothelium (Figure 1).

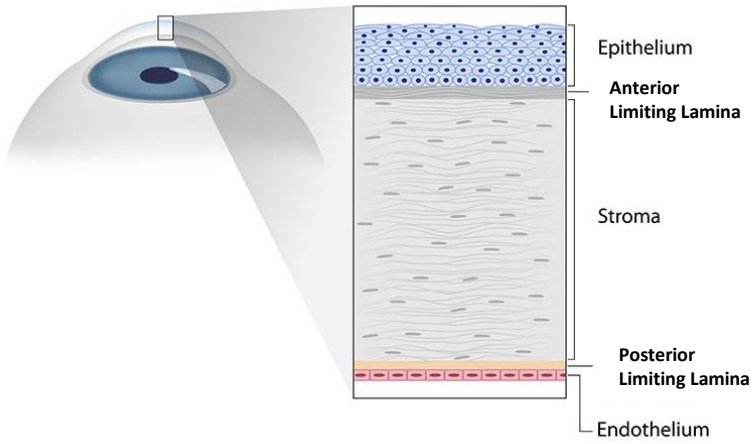

(Alila Medical Media, publicdomainpictures.net, Public Domain)

Figure 1. Illustration of the human corneal layers: epithelium, anterior limiting lamina, stroma, posterior limiting lamina, and endothelium

The epithelium, the most anterior layer, is a hydrophobic layer consisting of tightly packed, nonkeratinized, stratified squamous epithelial cells[1]. The human corneal epithelium is approximately 50 µm thick. The normal thickness of the corneal epithelium is maintained by ongoing mitosis and basal cell migration[3,4]. It is a renewable protective layer that serves as a barrier against environmental factors like microbes, UV light, and fluid. A healthy corneal epithelium does not contain white blood cells, however when injured or inflamed, the epithelium can be infiltrated by white blood cells[2]. The epithelium rests on a basal lamina which is secreted by epithelial cells. The basal lamina lies directly on top of the corneal epithelial basement membrane (BM)[5]. In general, basement membranes throughout the body are specialized extracellular matrices that function in anchoring adjacent cells and aid in regulation of cell adhesion and migration[5]. In the cornea, the epithelial BM functions to provide a physical barrier against the infiltration of

microbes into the stroma[6]. The anterior limiting lamina (ALL), or Bowman's Membrane, is directly beneath the basal lamina and epithelial basement membrane. The ALL, roughly 8-12 μm thick, is a nonregenerating layer that decreases in thickness with age[1]. It consists of dense, fine, randomly organized collagen fibers which form extensions into the anterior stroma[7,8].

The stroma, directly below the anterior limiting lamina, is the thickest layer of the human cornea (500 μm), comprising roughly 80-85% of its total thickness[9]. The stroma consists of highly organized collagen arranged in fibrils, predominantly type I collagen fibrils and fibrillin-1[10,11]. There are other lesser represented types of collagen (type IV, V, and VI) which provide additional support[12]. Furthermore, there is ground substance in the stroma which consists of glycosaminoglycans (GAGs), proteoglycans, and glycoproteins[13]. The bundles of collagen fibers within the stroma have a relatively uniform organization[12,14,]. The precise assembly and rigidity of this system, collectively called lamellae, has importance for the cornea's transparency, curvature, and resilience to shearing forces[15]. There are approximately 240 lamellae per stroma[16]. Within the stroma, there are resident cells including keratocytes (primarily), dendritic cells, and macrophages[12]. The posterior limiting lamina (PLL), or Descemet's membrane, is the underlying protective layer directly beneath the stroma. It is essentially the basement membrane of the endothelium. Its components are continuously secreted by the corneal endothelium throughout life, making the PLL the thickest basement membrane in the body[2].

The most posterior layer of the cornea, the endothelium, is a hydrophobic layer, consisting of a single layer of flat, hexagonal cells. The corneal stroma is hygroscopic, and the primary function of the endothelium is to provide corneal deturgescence by

pumping water out of the stroma to maintain a 78% water content which is optimal for transparency[14]. Excess accumulation of water in the stroma leads to increased separation between lamellae, resulting in edema and increased scattering of light[17]. The fluid movement between the cornea and aqueous humor involves Na+ K+ ATPase pumps and sodium bicarbonate. Pathophysiological events, such as the presence of guttae in Fuchs' endothelial dystrophy, compromise the endothelial pumps[18].Complete endothelial coverage of the posterior corneal surface is crucial for maintaining net water movement and thus corneal transparency[2]. The endothelium is partially permeable to ions for maintaining the osmotic gradient. Endothelial cells have junctional complexes including tight junctions, known as zonula occludens, found on the apical cellular sides which limit movement of fluid between cells[1,2]. Gap junctions are present along the lateral walls of the cells and function in communication rather than a physical barrier[19]. Intermediate junctions, zonula adherens, are located in between the cells and provide structural support by promoting cell-to-cell adherence[19]. Endothelial cells are non-renewable, and in the normal cornea endothelial density declines with age at a rate of 0.6% per year[20]. This rate of decline increases with ocular surgical trauma[20].

Being the most densely innervated structure in the body, the cornea contains sensory and autonomic nerves, originating predominantly from the trigeminal ganglion[21,22]. Virtually all mammalian corneas receive sympathetic innervation from the superior cervical ganglion, with varying inter-species innervation densities. In the mouse cornea, a single sensory neuron contains ~200 individual nerve endings[23]. The nerve fibers derive from the ophthalmic branch of the trigeminal nerve and enter the cornea from the periphery in a radial manner[24]. These nerve fibers are unmyelinated, and course through the central stroma, where they eventually divide into the subepithelial

plexus (anterior) and subbasal plexus (posterior)[24]. There are occasional interactions between nerve fibers and proximal keratocytes. Corneal nerves are also responsible for developing and secreting trophic factors necessary for maintaining the corneal epithelium. When these regulatory factors are released under “basal physiological conditions,” they stimulate corneal epithelial cells as a natural mechanism for tissue renewal[24].

Human Limbus

The limbus appears as a continuation of the corneal epithelium serving as a junction between the cornea and sclera. The limbus does not have its own tissue, rather it defines the border between the clear cornea and opaque conjunctival tissue. The cornea is avascular and must obtain nutrients from elsewhere; aside from the tears and aqueous, the peripheral cornea acquires nourishment from the limbus. Additionally, the limbus serves as a regenerative component in epithelial tissue, a pathway for aqueous humor outflow and as an incision landmark for cataract and glaucoma surgeries[25]. This narrow region contains radially oriented vascular, fingerprint-like ridges known as Palisades of Vogt that define a niche for stem cells, which are crucial to corneal epithelial renewal[26]. In addition to stem cells, the peripheral cornea contains various cell types including natural killer cells, keratocytes, platelets, and PMNs. Insult to the cornea will induce an inflammatory response resulting in PMN extravasation and migration into the cornea toward the site of injury or infection. Thus, one of the principal functions of the limbus is to serve as a vehicle for PMN delivery to the cornea to resist infection and provide efficient wound healing.

Though no precise boundaries define the limbus, several landmarks are clinically visible. Superficially, the connection of the corneal and conjunctival epithelia form the limbus. A shallow trough, known as the external scleral sulcus is seen at the transition zone between the cornea and sclera, where there is an abrupt change in the radius of curvature. The internal sulcus is formed by the scleral spur. Internally, the limbal region begins at the junction of the PLL, the endothelium and the most anterior extent of the trabecular meshwork, Schwalbe's line[25]. The basal lamina of the endothelium is continuous with the trabeculum as the modifications of the endothelial cells into trabecular cells form the trabecular meshwork, which plays an important role in aqueous outflow and intraocular pressure. This area of PLL-trabecular overlap has been increasingly studied, as interventions like a penetrating keratoplasty may induce an alteration of the elastic expression within the corneo-trabecular junction, causing a risk factor for development of glaucoma[27,28]. The limbus is defined differently histologically and pathologically. Histologically, the limbus is defined by the physical appearance of the junction of the cornea and sclera seen in a cross-section. Pathologically, the limbus is defined anteriorly by a demarcated line connecting the most peripheral points of the ALL and PLL, and posteriorly by a line from the scleral spur perpendicular to the tangential surface of the globe[25].

The limbal vasculature contains a rich capillary plexus which supplies the peripheral cornea, conjunctiva, sclera, episclera, and peripheral uvea. The arterial vessels are derivatives of the anterior ciliary arteries. From the episcleral arterial circle, there are two types of arterioles that arise: the first type of arteriole is the terminal branch that passes through the Palisades of Vogt, forming the limbal arcades or "limbal loops" that supply the peripheral cornea; the second type of arteriole is the redundant vessel

which contributes to the limbal arcades as well as traveling posteriorly to supply the anterior conjunctiva[29]. It is from the limbal vasculature that white blood cells extravasate and enter the extracellular tissue before migrating into the avascular corneal stroma[30,31].

The Mouse Cornea and Limbus as an Experimental Model

For decades, the mouse model has been appreciated for genetic engineering as well as for studying physiology and pathology of the anterior segment of the human eye. Compared to the human cornea, the mouse cornea is significantly smaller. While anatomical and structural differences exist between the two species, similarities in function still remain. For one, the mouse lens occupies a larger surface area of the posterior chamber, which contributes to the convex appearance of the iris[30]. The stroma is much thinner in the mouse cornea. The mouse stroma becomes thinner from central to peripheral areas while the human stroma thickens. In spite of the disproportionality in thickness, the structural organization of the stromal collagen fibers is very similar to that of the human cornea. Fibrillin-rich microfibril bundles which aid in maintaining corneal shape and tensile strength are present in both the mouse and human cornea[32]. However, the fibrillin-1 expression is more extensive within the mouse stroma. In the periphery, the human cornea contains true elastic fibers, while the mouse cornea lacks true elastic fibers and possesses tropoelastin, a precursor for mature elastic fibers[32]. A mouse cornea also lacks an anterior limiting lamina. The limbal vasculature of the mouse is much simpler compared to that of humans. In the mouse limbus, Schlemm's canal is linked to the superficial limbal vascular plexus directly via aqueous vessels, with only "the occasional simple plexus just superficial to Schlemm's canal"[33]. On the contrary, in the human limbus, collector channels connect to a deep scleral plexus. From

there, the aqueous veins lead to a midscleral plexus which finally drains to a superficial perilimbal plexus. Although the human limbal vasculature contains a more intricate pattern of aqueous vessels, the purpose of arteriovenous anastomoses in both mouse and human is suggested to remain the same, where they “act as shunts between arteries/arterioles and veins/venules,” provide flow resistance, and “may play a role in regulating the outflow of aqueous into the circulatory system”[33]. Other similarities exist in the corneal innervation. Both have peripheral stromal branches which develop into a sub basal plexus that join to form a “vortex” pattern in the central cornea. Both mouse and human corneas have lower stromal nerve density and higher epithelial nerve density in the central cornea[34]. Table 1 summarizes the anatomical differences between the human and mouse cornea.

Despite the challenges in research created by the differences between the mouse and human cornea, there are sufficient similarities to warrant its use as a model for human disease. The mouse corneal stromal structure and cellular function is similar to humans. Studies with various mouse strains show that after corneal epithelial debridement, mice undergo recurrent corneal erosions and exhibit similar wound healing rates to that of human corneas[35]. More interestingly, in that study the C57Bl/6 mouse strain exhibited the fastest rate of reepithelialization[35]. Collectively, the research reinforcing the similarities between human and mouse corneas support the use of the mouse model as a common and appropriate model for studying corneal regeneration and homeostasis.

Table 1. Summary of Human vs. Mouse Anatomy

	Human	Mouse
Cornea		
Epithelium	○ 50 µm central thickness ○ 5-7 layers	○ 40 µm central thickness ○ 10-13 layers
Anterior Limiting Lamina (Bowman's Layer)	○ 8-10 µm thickness	○ Undetermined lamina; not a distinct layer
Stroma	○ 500 µm central thickness ○ Thickens towards the limbus ○ Lamellar organization ○ Fibrillin-1 rich microfibrils ○ True elastic fibers	○ 65-90 µm central thickness ○ Thins towards the limbus ○ Lamellar organization ○ Fibrillin-1 rich microfibrils (more extensive) ○ Tropoelastin-no true elastic fibers
Posterior Limiting Lamina (Descemet's Membrane)	○ 2-20 µm thickness	○ 2-4 µm thickness
Endothelium	○ 5 µm ○ Single layer	○ 2-4 µm ○ Single layer
Diameter	○ Sclera surrounds cornea	○ Approximately the diameter of entire globe; 50% sclera
Lens	○ Occupies a lesser amount of the posterior chamber	○ Occupies a greater amount of posterior chamber
Iris	○ Nearly flat plane	○ Anteriorly bowed plane

Polymorphonuclear leukocytes

Neutrophils (PMNs) are a vital component of the innate immune system, being the most abundant white blood cell in most mammals. PMNs originate in the bone marrow and upon maturation enter the bloodstream and function as first responders to tissue insult or injury and are necessary for efficient wound healing. PMNs have long been considered as tissue-destructive cells involved in phagocytic uptake, intracellular destruction, and extracellular discharge of digested pathogens. However, recent studies suggest a more complex behavior pattern in which PMNs provide signals to activate the recruitment of other innate and adaptive immune cells including macrophages, T-cells, and B-cells[36,37,38]. PMNs are now emerging from their reputation as acute inflammatory responders to long-term regulators of the adaptive immune system.

PMNs undergo a process of aging within the living organism. The approximate half-life of PMNs in the circulation is 6-12 hours for mice and humans[39]. The short lifespan in circulation of PMNs, calls for a rapid development and release of PMNs, approximately 10^{10} PMNs per day from the bone marrow, and requires a balance between the “release-clearance” system[39,40]. Regulating PMN numbers in the blood is critical as too few PMN (neutropenia) can result in an increased susceptibility to infections, whereas too many PMNs (neutrophilia) may promote tissue damage leading to chronic inflammation[41]. PMNs age as they circulate, and a single blood sample will contain “fresh,” newly formed PMNs as well as “aged,” PMNs ready to be cleared from the bloodstream. Upregulation of surface chemokine receptor 4 (CXCR4) in fresh PMNs allows for better entry into the circulation and migration. Furthermore, downregulation of surface chemokine receptor 2 (CXCR2) in aged PMNs promotes their clearance from tissues[39].

In the non-adaptive immune response, following insult to the cornea, an inflammatory cascade is initiated to aid in restoration of the damaged cells. Because PMNs are the first responders during acute injury, they possess the ability to differentiate from a resting, circulating PMN to an inflammatory PMN and quickly reach the site of insult[42]. When recruited into extravascular tissue, PMNs undergo a phenotypical and functional transformation from a non-motile cell to cytokine-activated motile cell[41] (Figure 2). During the process, the cell acquires different surface markers and proteins, allowing for increased motility for the PMN to navigate to the site of recruitment[42]. Extravasated PMNs can have an increased lifespan of 24-48 hours, and this occurs through a delay in apoptosis, however, dysregulation of this process can lead to tissue damage[41,43].

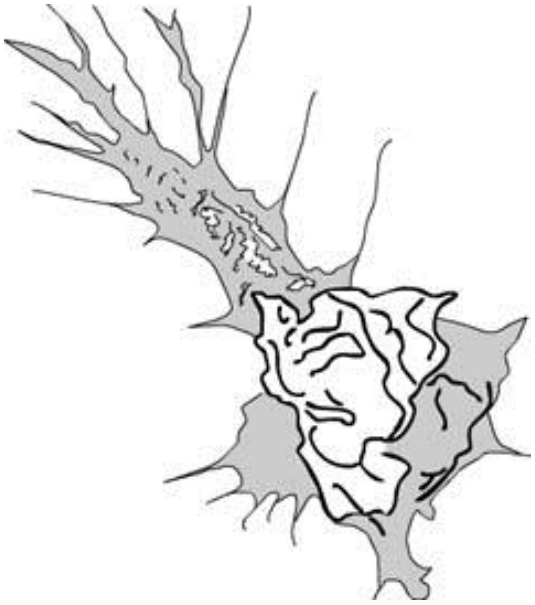

Figure 2: Extravascular polymorphonuclear leukocyte

(Image courtesy of Samuel Hanlon, O.D., Ph.D., *Neutrophil Interstitial Migration* 2012 (Doctoral Dissertation, University of Houston, Houston, US). pp.13.

An extravascular PMN undergoes a phenotypical change, allowing for efficient motility to migrate to a particular site of injury.

Differentiated PMNs within the vasculature exit the limbal vessels to migrate through an intricate path within the fibrous stromal tissue to access the remote site of injury[30]. To navigate through the dense, complex fibers and lamellae within the stroma, PMNs utilize adhesive, integrin-dependent interactions with the extracellular matrix and keratocytes[31]. PMNs preferentially migrate within the anterior stroma, making surface contact with keratocytes as they travel toward the injury. Contact with keratocytes is mediated by CD18 adhesion molecules, and it has been suggested that the keratocyte network serves as a cellular highway for efficient trafficking of PMNs[44]. PMNs are normally found in the flowing blood stream and not attached to the vascular endothelium. When the vasculature becomes inflamed, PMNs form loose attachments to the endothelium using selectins on the endothelial cells and the glycoproteins and L-selectins on the PMN[45]. The affinity for the vascular endothelium is low enough to be broken by shearing forces of blood circulation, causing the PMN to break free from the bond and tumble along the endothelial vessel. However, inflammation also triggers the production of chemotactic factors (e.g., interleukin-8) that bind to the endothelial surface, and when a rolling PMN encounters the surface-bound chemoattractant, the rolling PMN becomes activated and arrests on the endothelial surface. Arrest is facilitated by the interaction between PMN CD18 adhesion molecules and endothelial intercellular adhesion molecule-1 (ICAM-1)[45]. The binding of the chemoattractant results in a conformation change in the PMN CD18 adhesion molecules that results in a high affinity state for CD18 favoring ICAM-1 binding. Other interactions with cytokines and platelets within the endothelial wall further increase the affinity of the PMN to the endothelium and cause it to roll along the blood vessel[46]. Once the PMN firmly adheres to the endothelium via its CD18 interaction with ICAM-1, adhesion molecules PECAM-1, JAM,

and CD99 assist in the extravasation of the PMN[45]. Extravasated PMNs clear the pathogens if they are present and release inflammatory mediators and growth factors necessary for tissue repair. A good example, is the VEGF-A release from extravasated PMNs which promotes efficient nerve recovery after a corneal abrasion[47].

There is mounting evidence from studies in other tissues that PMN extravasation can also occur in the absence of overt inflammation. Specifically, when aged PMNs leave the circulation and migrate into tissue their functionality is altered[39]. Clearance and migration of aged PMNs from the bone marrow differentiates the PMNs where they perform specialized functions. For example, an aged PMN cleared from the bone marrow migrates to the spleen or liver allowing for B-cell support or metabolic regulation, respectively. Aged PMN clearance in the bone marrow functions as a regulator of the hematopoietic niche, which is the primary regulator of HSPC creation[39, 48]. Additionally, the research shows that PMNs' aging follows a temporal fluctuation during its lifespan, from "fresh" to "aged," which correlate with the patterns of incidence of infections from pathogens in the environment[49]. Circadian rhythms are present within parasites where they display rhythms in their reproductive cycle within and release from their hosts[49]. Since there is a synchronization of the biological rhythms with the circadian rhythm of PMNs, it would be of importance to study the temporal regulation of PMNs.

Circadian Rhythm

Circadian rhythm, termed from the Latin *circa diem*, meaning 'for about a day,' describes an organism's internal time clock that roughly coincides with the earth's rotation cycle[50]. Circadian rhythms have a powerful influence over physiological and pathological events, controlling roughly 10% of the mammalian genome. Circadian

rhythms allow living organisms to adapt to environmental changes as well as provide an internal protective mechanism by separating incompatible processes in the body like catabolism and anabolism. The alignment of an organism's internal time clock with an external clock is termed entrainment. Zeitgeber (ZT) meaning "time giver," is a German term given to describe an environmental cue, e.g. light or temperature that aligns the endogenous clock with the external circadian rhythm. In most cases, light is the factor that sets the "rest-activity cycle" of an organism[50]. The endogenous circadian rhythm is present globally as well as locally where it is noted that there are "tissue-specific oscillations" in the recruitment of adhesion molecules and chemokines. These oscillations are coordinated to match with the expressions of pro-migratory factors that increase the accumulation of immune cells during various times in the circadian cycle, consistent with circadian rhythms acting as a protective mechanism[50].

It has previously been understood that PMNs are summoned by an inflammatory cascade of events via local modulators at the site of injury or infection. In recent studies, Scheiermann and colleagues observed recruitment of PMNs in the absence of overt inflammation and determined this recruitment was influenced largely by adrenergic nerves and the sympathetic nervous system[51]. In the mouse, this method of recruitment of PMNs to tissues is regulated by distal, long range signals and follows a circadian pattern, where peak recruitment is at night when the mice are active. The rhythmic recruitment of PMNs is noted in vital organs including the bone marrow and skeletal muscle[39].

PMNs are a rich source of growth factor VEGF-A, which is essential for corneal nerve regeneration in wounded corneas[47]. Our laboratory showed that following corneal epithelial abrasion in the mouse, PMNs and platelets are recruited into the extravascular

space via a γδ T-cell-dependent inflammatory cascade. IL-17 acts as a chemoattractant that attracts peripheral neutrophils to the site of injury. PMNs migrate even further into the central cornea within hours of the insult. Peak levels of PMN-derived VEGF A coincided with peak tissue levels of PMNs. PMN extravasation and the release of VEGF-A is necessary for efficient nerve recovery in the wounded mice with ~19% regeneration of sensory nerves within 96 hours. Conversely, γδ T-cell-deficient mice or mice treated with anti-IL-17 have ">50% reduction in leukocyte and platelet infiltration and >50% reduction in nerve regeneration"[47].

Metabolic syndrome

Metabolic syndrome is a disease identified as a collection of conditions including dyslipidemia, elevated blood pressure, excess abdominal fat, and high fasting glucose levels. Obesity, defined as an excess accumulation of body fat, is one of the collective disorders in metabolic syndrome that increases the risk of cardiovascular disease and type 2 diabetes. One of the leading factors resulting in obesity, and in turn metabolic syndrome, is the consumption of a high fat diet. Metabolic syndrome is a leading cause of neuropathy, and in its early stages leads to structural and functional changes in the cornea (unpublished data, Burns *et.al*). Metabolic syndrome is associated with reduced corneal sensitivity. In a mouse model of diet-induced obesity (DIO), a loss of corneal nerve density and function are detectable after only a few weeks on the diet (Figure 3) (Burns et al., unpublished data, 2019). Corneas collected at 5, 10, or 15 weeks of HFD exhibited reduced corneal nerve density (number of vertical nerves or sub-basal nerve length). As stated earlier, published data suggest there is a circadian trend in PMN accumulation at the limbus when mice are fed a normal diet. In our preliminary studies, corneal circadian

expression of a clock gene, *Rev-erb alpha,* is blunted when mice are fed a HFD (Figure 4). The data show that a circadian rhythm is present in corneas and is altered in injured corneas (HFD).

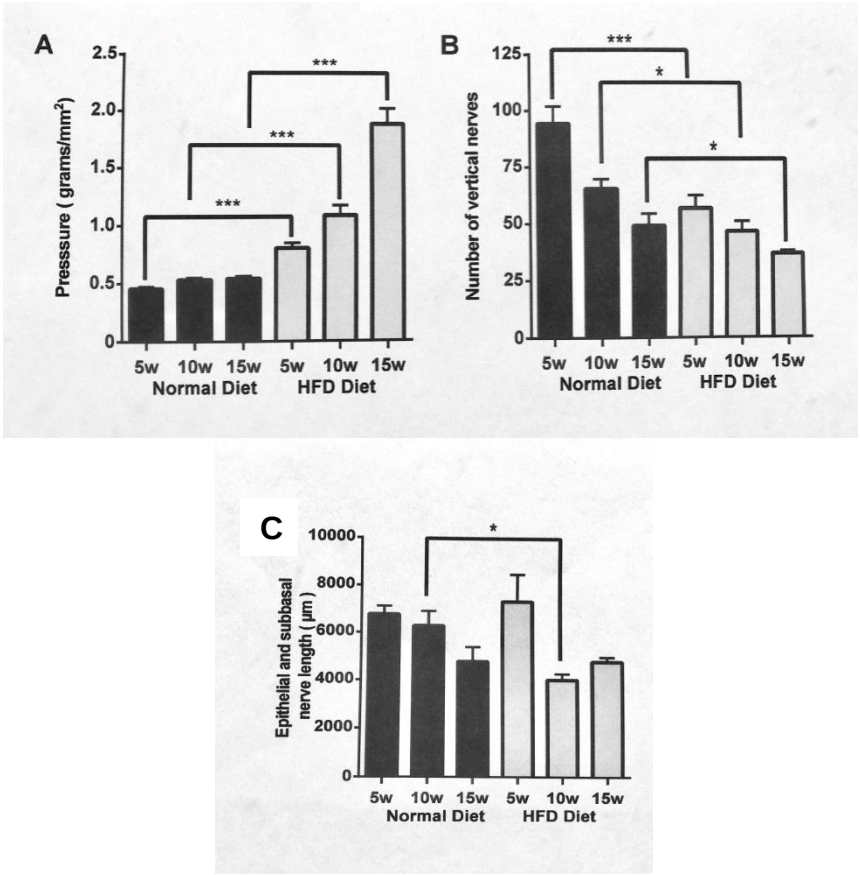

Figure 3. Corneal nerve changes may result from diet-induced obesity

Mice fed HFD showed reduced corneal sensitivity and density, and was most affected at 15 weeks on HFD. (A) The pressure necessary to induce a blink response. (B) Morphometric analysis of the number of vertical nerves observed by focusing in the epithelium (mid plane). (C) Analysis of length (µm) of nerves throughout the epithelium

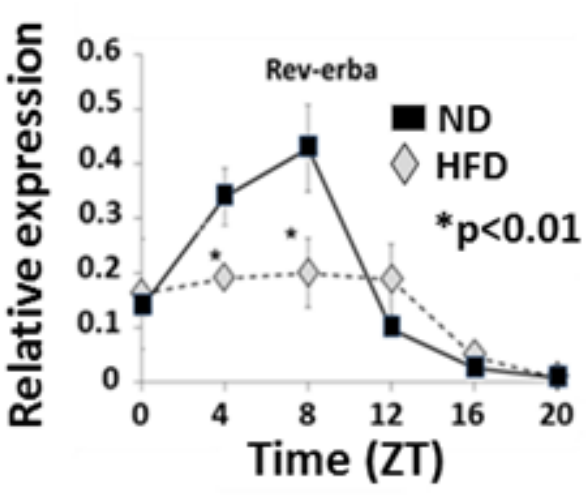

Figure 4. HFD suppresses corneal expression of Rev-erb alpha

Mice fed a normal diet showed a circadian pattern of Rev-erb alpha corneal expression while mice fed a HFD showed a blunted Rev-erb alpha expression.

There has also been a higher incidence of Type 2 diabetes diagnosed in the nation, with a CDC report in 2010 indicating that approximately 33% of U.S. adults over 19 years of age were pre-diabetic (Centers for Disease Control and Prevention 2013). Obesity in children has become more significant in the past several decades. Early disease detection is critical to successful treatment of the patient. It is important to detect adverse changes in diseases before they become detrimental. While the presence of retinopathy is a hallmark feature of Type II diabetes, considerable tissue damage to the retina and other organs in the body has already occurred. Importantly, 70% of diabetics exhibit keratopathy and, in the mouse, loss of corneal sensitivity seems to precede the development of insulin resistance and hyperglycemia (unpublished data). With the rising nationwide epidemic of obesity and Type II diabetes, it is important to have a better understanding of PMN accumulation at the limbus because of its potential role (e.g., VEGF release) in normal corneal nerve homeostasis because alterations in circadian rhythms may contribute to corneal nerve pathology.

Summary and Objectives

In summary, the evidence supports that PMNs, a crucial component in the immune response, are often present in extravascular tissues in unperturbed situations. As discussed earlier, PMNs are present at the murine limbus of the uninjured cornea. PMN migration into other uninjured tissues like the lungs and liver show a circadian pattern. Following a corneal injury, PMN recruitment is γδ T-cell-dependent and PMNs are necessary for corneal nerve regeneration. Interventions which diminish normal, non-inflammatory PMN accumulation at the limbus, like diet-induced obesity correlate with decreased corneal nerve density and function.

The **main objective** of this thesis is to evaluate whether a circadian flux of PMN infiltration is evident in an uninjured murine cornea. The **working hypothesis** is that a circadian pattern of PMN accumulation at the limbus is necessary for corneal homeostasis and that disruptions to this circadian pattern, like diet-induced obesity, are associated with corneal pathology involving nerve degeneration. While the exact function of these PMNs is unknown, it would be a possible path forward for future research.

To begin testing this hypothesis, the following **specific aims** were proposed:

Aim 1 will determine if there is a circadian flux of PMN extravastion at the limbus in the uninjured cornea.

Aim 2 will determine if consumption of a HFD affects PMN extravasation at the limbus.

Chapter 2: Materials and Methods

2.1 Sources of Materials

2.1.1 Animals

2.1.2 Diet Composition and Feeding Schedule

2.2 Tissue Processing

2.3 Immunolabeling and Processing of Slides

2.4 Fluorescence Imaging

2.5 Specifics for Enumeration of PMN

2.6 Statistical Analysis

Chapter 2: Materials and Methods

Studies were carried out at CNRC (Children's Nutrition Research Center) vivarium facility at Baylor College of Medicine (Houston, TX). The C57Bl/6 mouse model (7-12 weeks old) was used in all experiments. All animals were treated following the guidelines described in the Association for Research in Vision and Ophthalmology Statement for the Use of Animals in Vision and Ophthalmic Research and Baylor College of Medicine Animal Care and Use Committee Policy.

2.1 Sources of Materials

Animals

Male control C57Bl/6 wild type mice were purchased from Jackson Laboratory (Bar Harbor, ME). Mice were placed on a 12-hour light/dark cycle (6 AM/6 PM). The light/dark cycle (6AM/6PM) was performed as follows: at 6 AM lights were turned on to initiate the light cycle and at 6 PM lights were turned off to initiate the dark cycle. Four separate experiments were performed and at the end of each experiment, mice were euthanized by CO_2 asphyxiation or isofluorane inhalation overdose, followed by cervical dislocation according to IACUC guidelines. Whole eyes were enucleated and fixed in phosphate buffered saline (PBS, pH 7.2) containing 2% paraformaldehyde for 60 minutes at room temperature prior to rinsing and storing in cold (4^0C) PBS.

Diet composition and feeding schedule

Four distinct experiments were performed and in each case, C57Bl/6 mice (7 weeks of age) were fed for 10 days *ad libitum* (ad lib). For each of the four experiments, the mice were fed a normal chow diet (ND: 14.9% kcal fat, 64% kcal carbohydrate, 21%

kcal protein; Advanced Protocol PicoLab Select Rodent 50 IF/6F 5V5R, LabDiet, St. Louis, MO). In experiment 4, and additional group of mice received a high fat milk diet (HFD: 42% kcal milk-fat, 30% kcal sucrose, 11.8% kcal carbohydrate, 15.2% kcal protein; Diet #112734, Dyets Inc., Bethlehem, PA). The duration of the feeding was selected based on studies in our lab showing that mice exhibit decreased corneal nerve sensitivity following consumption of HFD after 10 days[34].Female mice were not used in this study because they do not develop the metabolic syndrome when given a HFD. Conversely, male mice of this strain have been shown to consistently become obese and exhibit metabolic syndrome within 5 weeks on the high fat diet[52,53].

Tissue Processing

Fixed enucleated mouse eyes were dissected under a microscope by making an equatorial incision and removing the full cornea. The lenses were then removed and the iris pigment was scraped away from the anterior segment. Prior to immunolabeling, four radial incisions were made on each cornea running from the peripheral to paracentral cornea so that the immunolabeled cornea would lie flat when placed on the plane of a glass slide. Corneas were permeabilized with PBS containing 0.1% Triton X-100 for 15 minutes and then blocked with PBS containing 0.1% Triton X-100, 2% bovine serum albumin (BSA), and Fc blocker overnight at 4^0C prior to immunolabeling.

Immunolabeling and preparation of slides

Permeabilized and blocked corneas with limbus intact, were incubated with PBS containing 2% BSA containing fluorochrome-conjugated antibodies: anti-Ly6G (BD Pharmingen, San Jose, CA) for detection of neutrophils and anti-CD31 (BD Pharmingen, San Jose, CA) for detection of blood vessels (Figure 6). For detection of cell nuclei, 4', 6-diamidino-2-phenylindole (DAPI; Sigma Aldrich) was used. Immediately prior to immunolabeling, antibodies were centrifuged (13,000xg, 2 minutes) to remove IgG aggregates. Table 2 summarizes the concentrations of each antibody prepared for each experiment. Immunostained corneas were mounted on microscopic slides and covered with Airvol 205 mounting media (Sigma-Aldrich Corp., Celanese, Dallas, TX). The prepared slides were covered with 1.5 um coverslips and 2.72 gram-weights were placed centrally above the coverslips. Slides were allowed to lay flat in a dark area for 24-48 hours at room temperature. After the drying process, slides were stored upright at 4^0C.

Table 2. Fluorescent Markers

Fluorescent markers (DAPI and antibodies) for labeling corneas in experiments 1-4.

Cell Marker (vendor)	**Excitation/Emission maxima (nm)**	**Target**	**Concentration used**
4',6-diamidino-2-phenylindole (DAPI) (Sigma Aldrich, D8417-10MG)	360/460	Chromatin	1 µg/ml
Rat anti-mouse Ly-6G, Alexa Fluor 488 (Invitrogen, #RM3020)	495/519	Neutrophils (clone: RB6-8C5)	10 µg/ml
Rat Anti-mouse CD31 (PECAM-1), APC (BD Biosciences, #551262)	650/660	Blood vessels (clone: MEC13.3)	5 µg/ml

Fluorescence Imaging

Across all experiments, images were captured using a DeltaVision Core Spectris inverted fluorescence microscope (Applied Precision, Issequah, WA). One image was taken of one of four radial cuts of the cornea on one microscopic slide. To capture images of the limbus, a 10X dry objective lens was used to capture sections of the mounted cornea on the microscope slide to view nuclei, blood vessels, and neutrophils. Images were stitched to form multipanel images to visualize the entire limbal vasculature of one of the four radial petals. The image was then deconvolved. Digital z-stack images (0.3 um/slice) were obtained encompassing the full thickness of the cornea. A maximum intensity image projection was then used to combine all deconvolved sections into a single two-dimensional 1024 x 1024 image. Deconvolution and projection of the images were made using SoftWorx software. The final stitched images were analyzed using Image J software. All images were captured under identical exposure conditions.

Specific Methods for Enumeration of PMNs

PMN Enumeration

Images could be switched between red and green channels to observe solely neutrophils or solely blood vessels (Figure 6). PMN counts were made at the limbus region, pre-determined by the area of capillary loops on the central side and the descending branches draining venules from the peripheral side (Figure 6). PMNs that overlapped the vasculature were considered to be inside the vessel and were not counted. There were two observers for each corneal count. For experiment 1, PMN counts were obtained by the use of transparency papers laid over projected computer image of the files of equal size. An observer would count PMNs in groups of five, and

circle groups with markers on the transparency paper. For experiments 2, 3, and 4, for the purpose of calculating PMNs per limbal area (mm^2), enumeration was performed with ImageJ software. A custom ImageJ software program was used to calculate the limbal areas of the region sampled, and counts would be displayed as PMNs/ mm^2. The analysis of 65 mouse corneas was performed by two independent observers. Each observer was masked to the identity of the captured images.

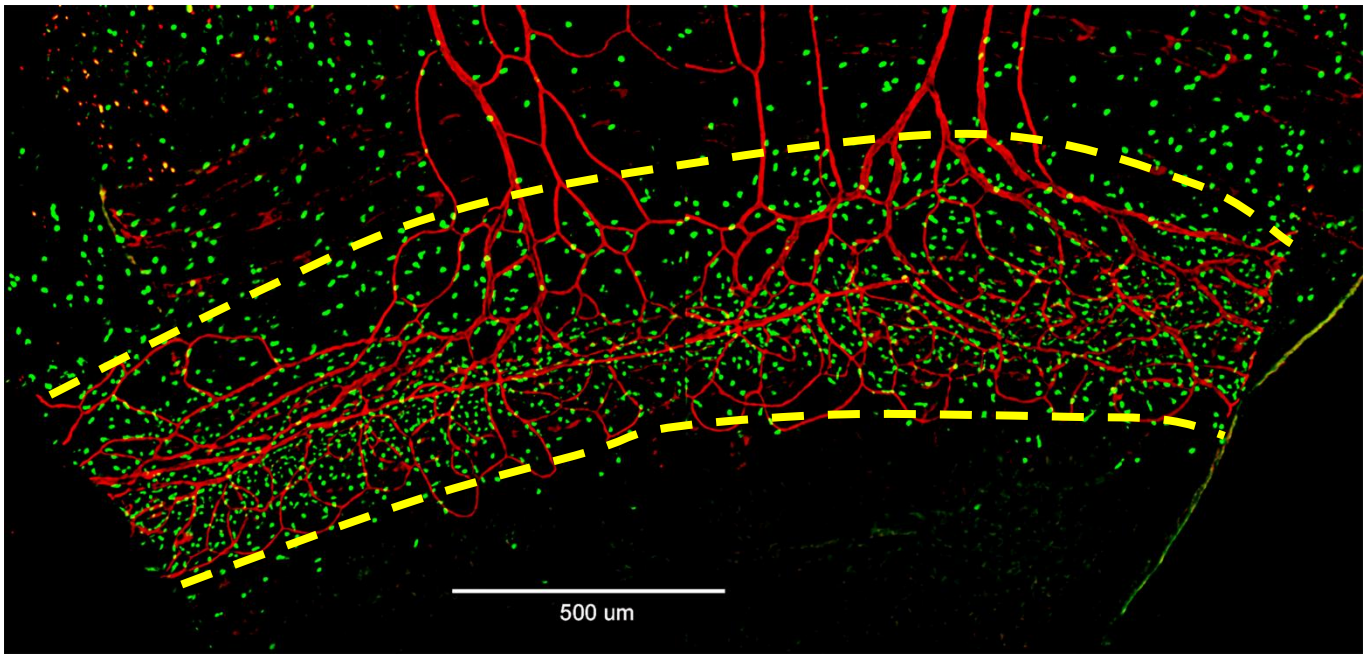

Figure 5. Extravascular PMNs in the nasal region of the limbus at 12 AM

In this example, yellow dashed lines show the limbal boundaries. This nasal quadrant has 1287 extravascular PMNs.

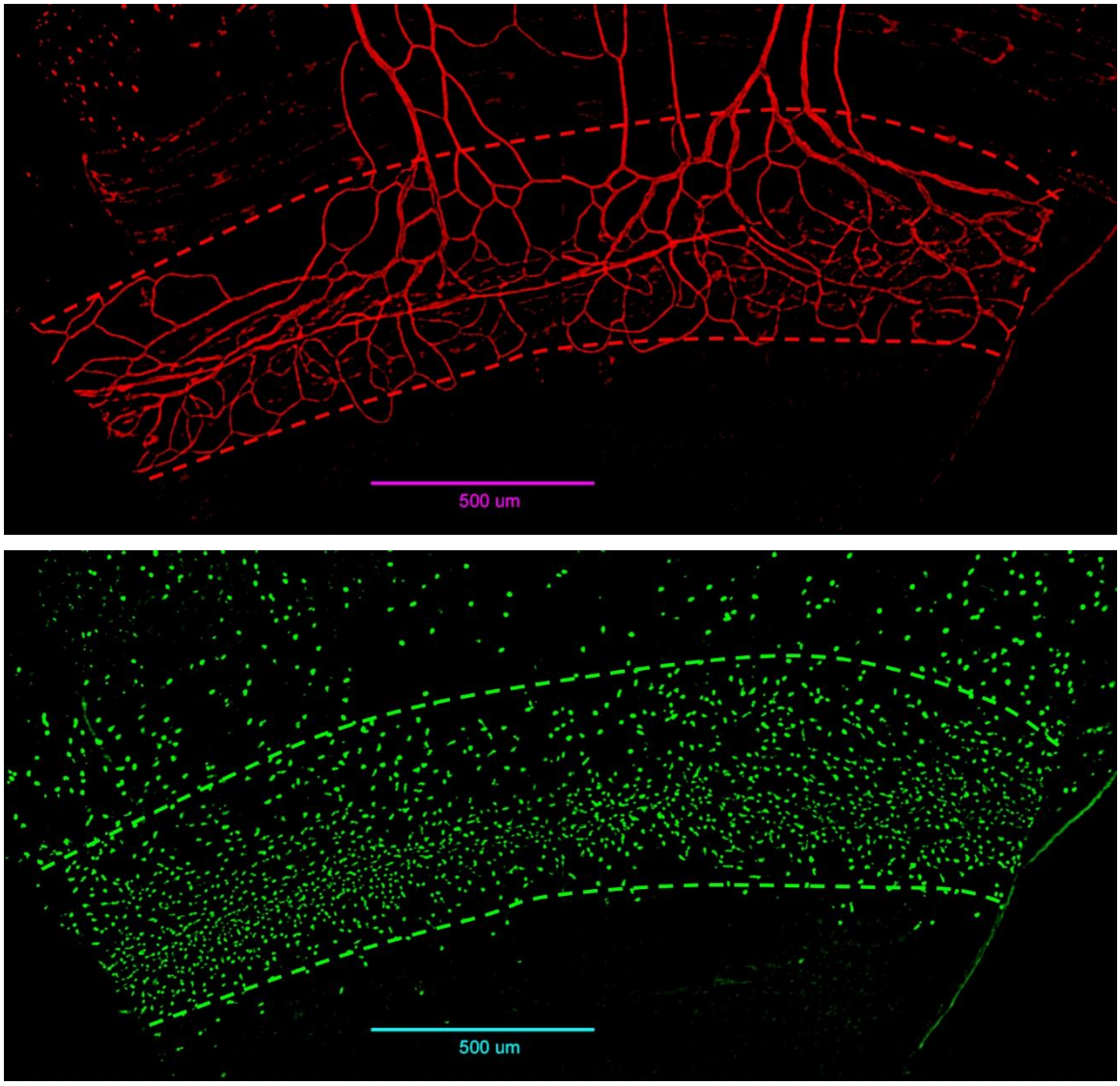

Figure 6. Utilizing two excitation/emission channels to view vasculature and PMNs

In this example, the image shown in Figure 5 has been split into two separate excitation/emission channels to better distinguish the vasculature from the PMNs. (A) Vasculature is clearly visible using the far red filter combination; corneas were labeled with anti-CD31 conjugated to APC (B) PMNs are visible using the FITC filter combination

Electrocautery

For experiment 1, we wanted to determine whether there was a difference in PMN extravasation across the four quadrants. To accomplish this, just prior to enucleation of the euthanized mouse, an electrocautery mark, approximately 0.35 mm diameter in size was burned onto the cornea located paracentrally from the cornea, approximately 0.5 mm away from the limbus in the superior aspect of the cornea.

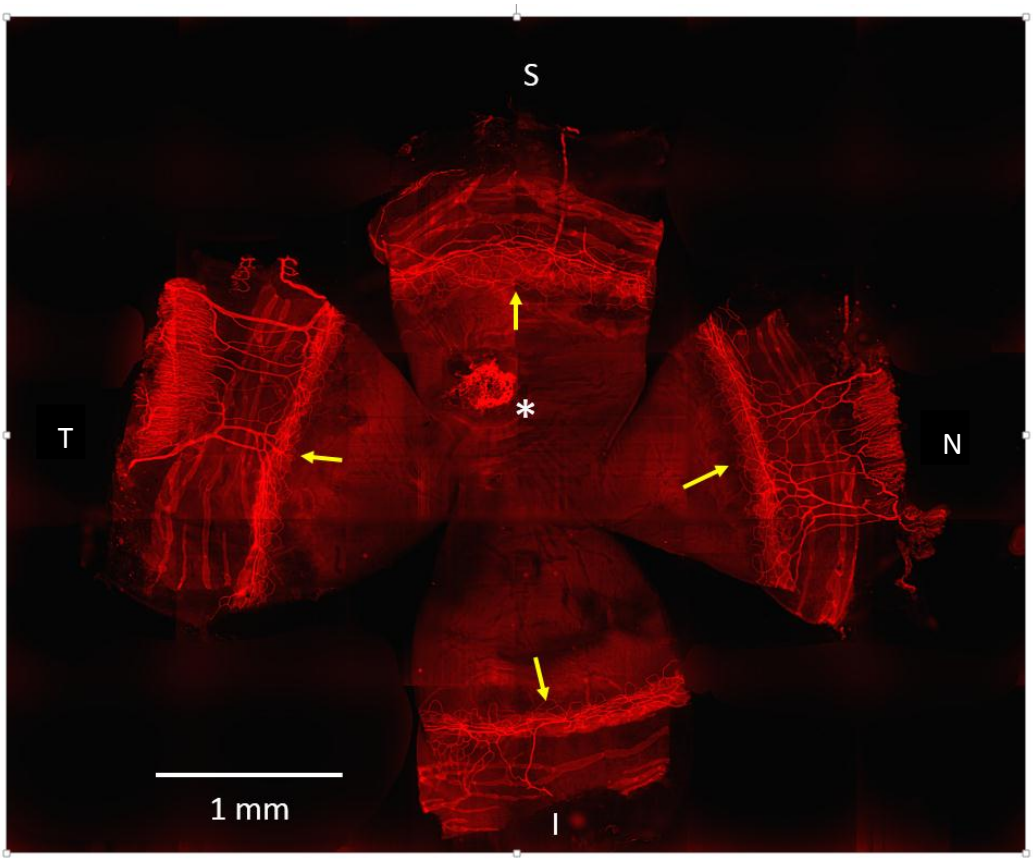

Figure 7. Limbus in the flat-mounted cornea from the left eye

Limbal vessels (arrows) labeled with anti-CD31 and the superior aspect of the cornea has been marked using electrocautery (*) such that the four quadrants (superior (S), nasal (N), temporal (T), and inferior (I) could be identified. Note the inversion of the image taken with a fluorescence microscope.

Adjustment for Radial Cuts

It was not always possible to obtain 1) radial cuts of exactly equal lengths and 2) radial cuts which include the electrocautery mark at the exact location on the superior aspect of the cornea. Figure 8 shows example images of two petals, one with an electrocautery mark in the exact center and off center. We ideally wish to have perfectly even radial cuts, obtaining equal lengths of each quadrant (superior, nasal, inferior, temporal), with the electrocautery mark in the exact center of the superior petal. Most of the time this did not occur. To achieve a better representation of PMN counts per each quadrant, calculations were made for redistribution of the anatomical quadrants within the flat mounted cornea (see Figures 9 and 10). The redistributions would assume equal lengths of each quadrant and that the electrocautery mark was made at the exact location of the superior aspect of the cornea prior to enucleation.

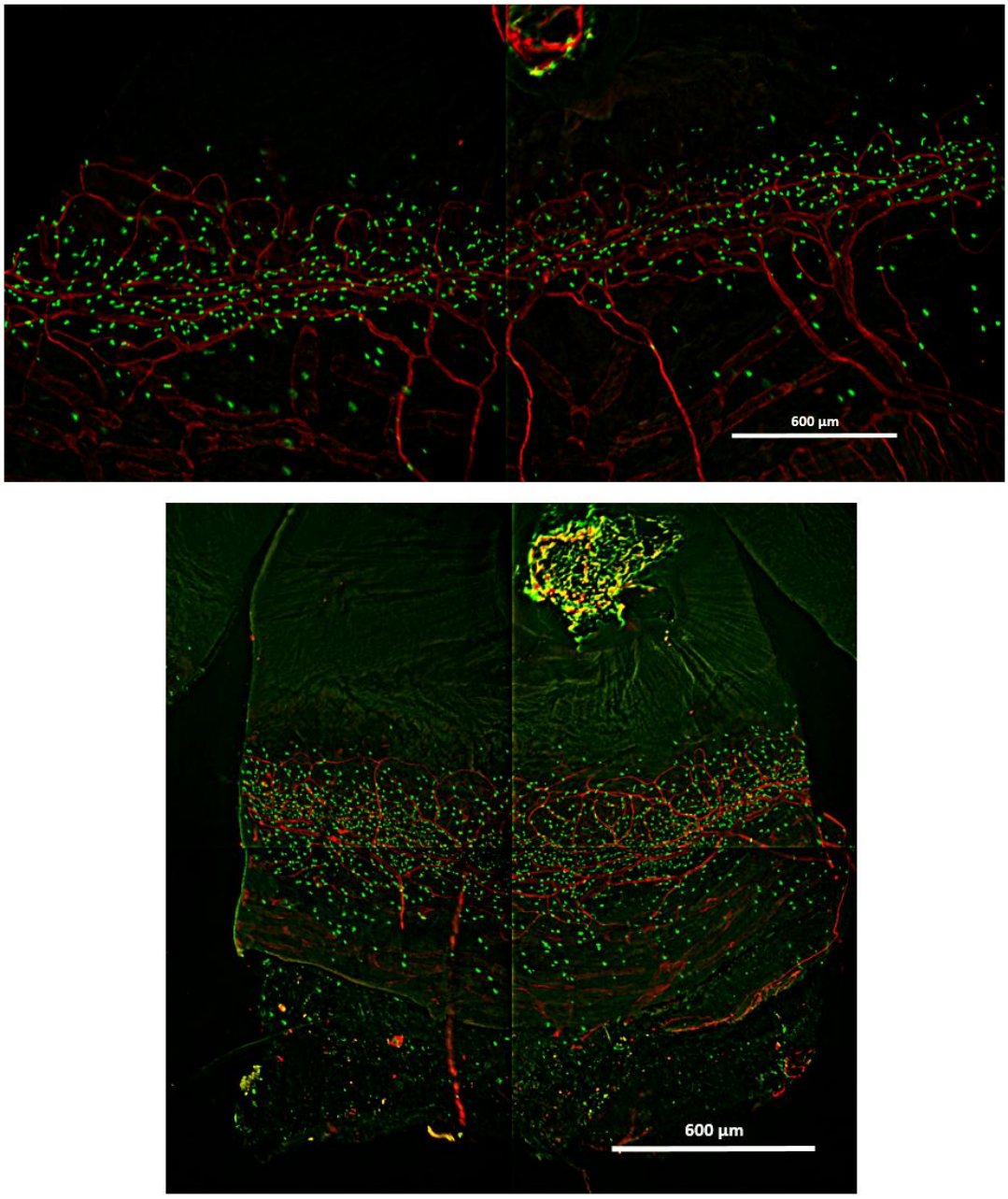

Figure 8. Two examples of electrocautery to label superior quadrant, showing equal radial cuts and unequal radial cuts

A) An example with radial cuts that result in the electrocautery mark in the exact center of the superior quadrant. B) a flat-mounted cornea with uneven radial cuts, resulting in the electrocautery mark on the edge. The examples shown are the superior quadrants of one radial cut from a flat mounted cornea from two separate corneas

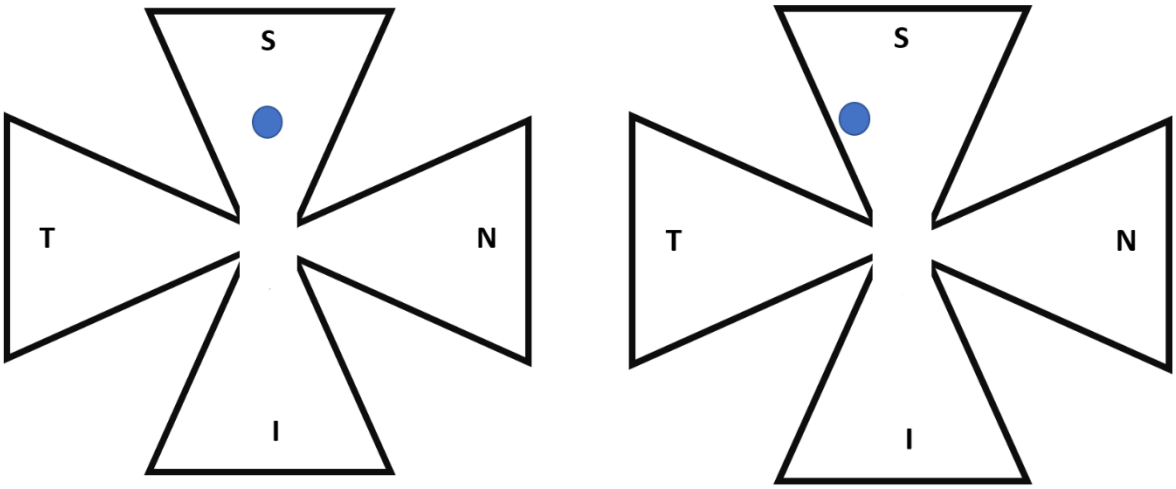

Figure 9. Schema demonstrating flat mounted corneas with radial cuts that result in a centered or off-centered electrocautery mark

A schematic diagram showing A) a flat-mounted cornea with radial cuts that result in the electrocautery mark in the exact center of the superior quadrant; B) a flat-mounted cornea with uneven radial cuts (figure not drawn to scale), resulting in the electrocautery mark on the edge (off-centered) of the superior quadrant.

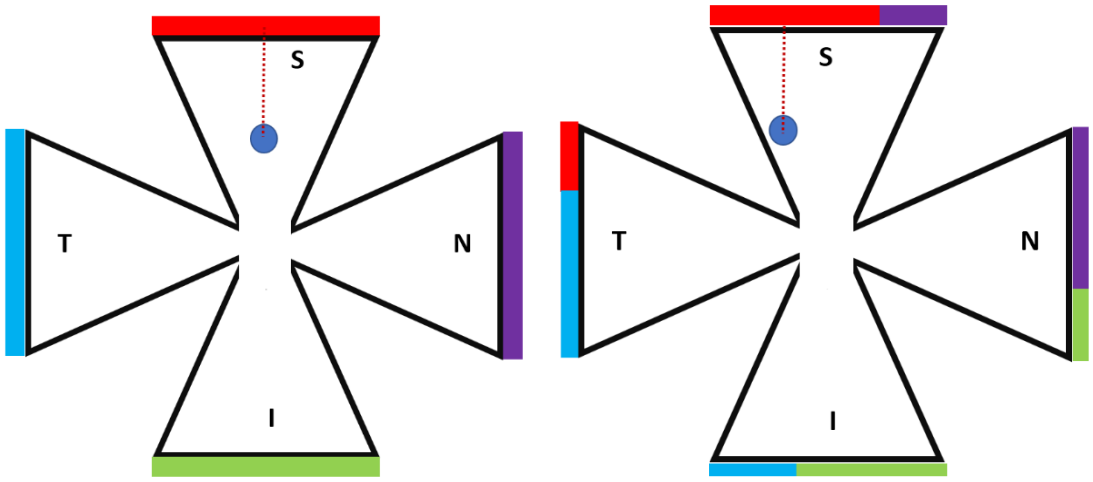

Figure 10. Schema showing flat mounted corneas with redistribution of the quadrants

A schematic diagram showing A) an ideal flat-mounted cornea with exactly equal radial cuts with the electrocautery mark (blue circle) centered directly on the superior petal. Each petal is equally represented by color (red: superior (S), purple: nasal (N), green: inferior (I), temporal (T)); B) a flat-mounted cornea with non-optimal radial cuts, where one makes calculations to redistribute the quadrants. Red dotted line indicates an extrapolation from the electrocautery mark to the limbus to demarcate the center of the superior quadrant. Figure is not drawn to scale.

Statistical Analysis

Data are summarized as mean ± standard error of the mean, with probability (p) value considered significant if ≤0.05 (with an exception in experiment 1, see below). Data collection was documented and organized in spreadsheets using Microsoft Excel 2013 software (University of Houston). Calculations and tests for significance were performed and graphs were produced using GraphPad Prism 8 software (GraphPad Software, Inc., La Jolla, CA). For experiments 1-3, PMN counts were obtained by two separate observers, and to determine the degree of agreement between observer's count, a goodness of fit linear regression model was developed to determine a correlation coefficient. Once agreement between observers was confirmed, subsequent statistical analyses were taken from Observer 1 data. (There was one observer for experiment 4). Data analysis was performed using a one-way ANOVA, two-way ANOVA (with Tukey posthoc-tests), or an unpaired t-test with equal variances.

Experiment 1

A one-way ANOVA was performed to compare means of PMN counts across eight time points (6 pm, 9 pm, 12 am, 3 am, 6 am, 9 am, 12 pm, 3 pm) with n=3 per time point. PMN counts were analyzed by two independent observers. To determine whether there was a difference between highest counts at 9 PM and lowest counts at 12 PM, an unpaired t-test was performed. Eight separate chi-squared tests were performed (one for each time point) to determine whether PMN extravasation was different between each quadrant (4 classes: superior, nasal, inferior, temporal) (GraphPad QuickCalcs Software). The differences in anatomical region preference were expressed qualitatively using a relative frequency graph. A power calculation was performed with a two-tailed statistical

significance (α=0.05) with an 80% power to determine the group size of animals to be used for this experiment.

Experiment 2

An unpaired t-test with equal variances was performed with a focus on determining a difference in PMN extravasation between evening (9 PM) and morning (12 PM) counts.

Experiment 3

An unpaired t-test with equal variances was performed with a focus on determining a difference in PMN extravasation between evening (9 PM) and morning (12 PM) counts.

Experiment 4

A two-way ANOVA was performed to compare the mean differences between two independent variables (time points: 11 PM and 11 AM; and diet: ND and HFD) to determine if there was a significant difference between PMN counts. Additionally, two separate unpaired t-tests with equal variances were performed to determine if there was a significant difference between 11 PM and 11 AM counts for ND and between 11 PM and 11 AM counts for HFD.

Pooling of data

Pooling of data from experiments 1-4 (mice fed a normal diet) was done to increase the sample size (n=18-19) (See Results). An unpaired t-test with equal variance was performed to determine if there was a difference in PMN extravasation between the pooled samples from evening (9 PM and 11 PM) and morning (9 AM and 11 AM) PMN counts.

Chapter 3: Results

3.1 Overview of Data Collection
3.2 Experiment 1
3.3 Experiments 2-4
3.4 Experiment 2
3.5 Experiment 3
3.6 Experiment 4
3.7 Pooling of Data

Overview of Data Collection

All data gathered in this study were from uninjured corneas obtained from C57Bl/6 male mice fed either a normal diet or a high fat diet. During the course of this study, 184,200 PMNs were counted from 233 mm^2 of corneal limbus imaged from 65 mice.

Experiment 1: Extravascular PMN counts showed a peak and nadir over a 24-hour period

Since PMN extravasation has been shown to have a circadian pattern in other uninjured tissues like the spleen and liver[39], we wanted to determine whether there is a circadian flux of PMNs in an uninjured mouse cornea. We first examined mice on a normal diet placed on a 12-hour light/dark cycle and collected corneas at 3-hour time intervals over 24 hours (6 pm, 9 pm, 12 am, 3 am, 6 am, 9 am, 12 pm, 3 pm). While a graph of the data (Figures 11 and 12) suggested extravascular PMNs in the uninjured mouse cornea were elevated at 9 PM (1089 ± 636.66) and lower at 12 PM (307 ± 88.87), the PMN counts were not significantly different (p=0.07).

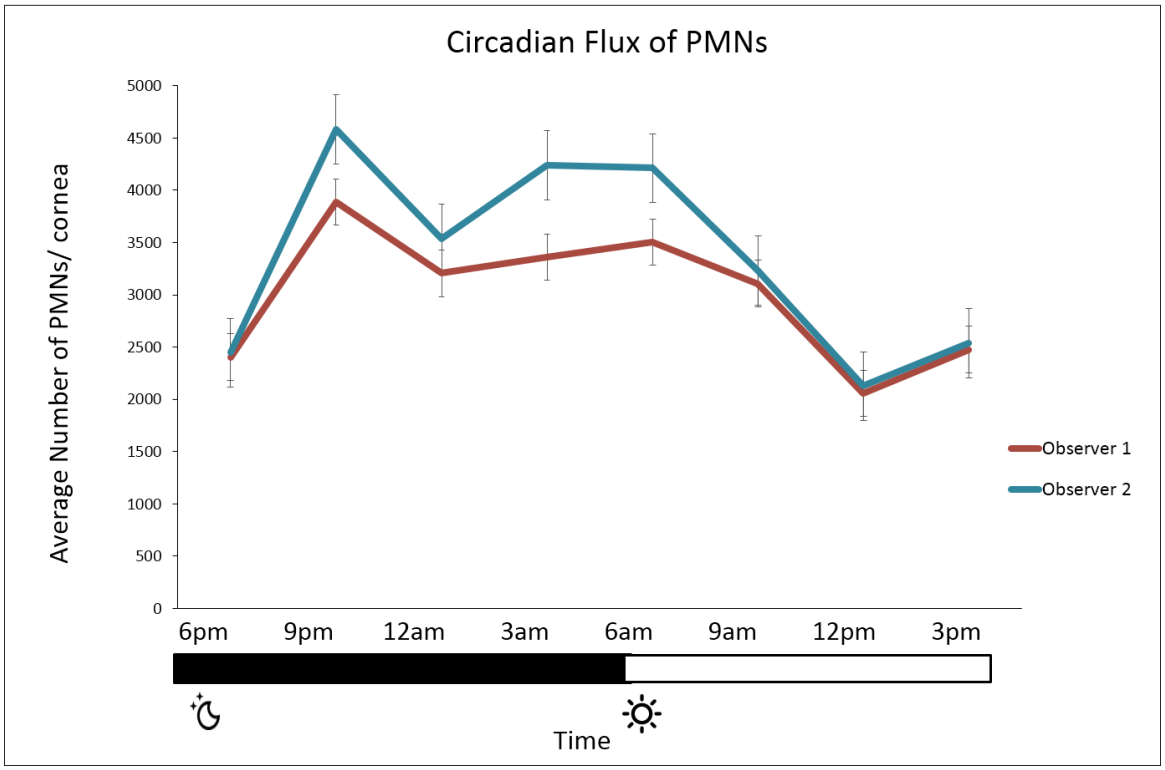

Figure 11. Extravascular PMN counts at the limbus in the uninjured mouse cornea during a 24h period.

Extravasation of PMNs were observed at 8 time intervals during a 24h period. Mice (n=3; mean per time point) were euthanized every three hours and corneas were immunostained for PMNs (see Methods for details). PMN counts are expressed as an average of 3 corneas for each time-point. Total PMN counts across 24 h period was made by two observers (Observer 1: red; Observer 2: blue). The degree of agreement between the two observers' data are shown below.

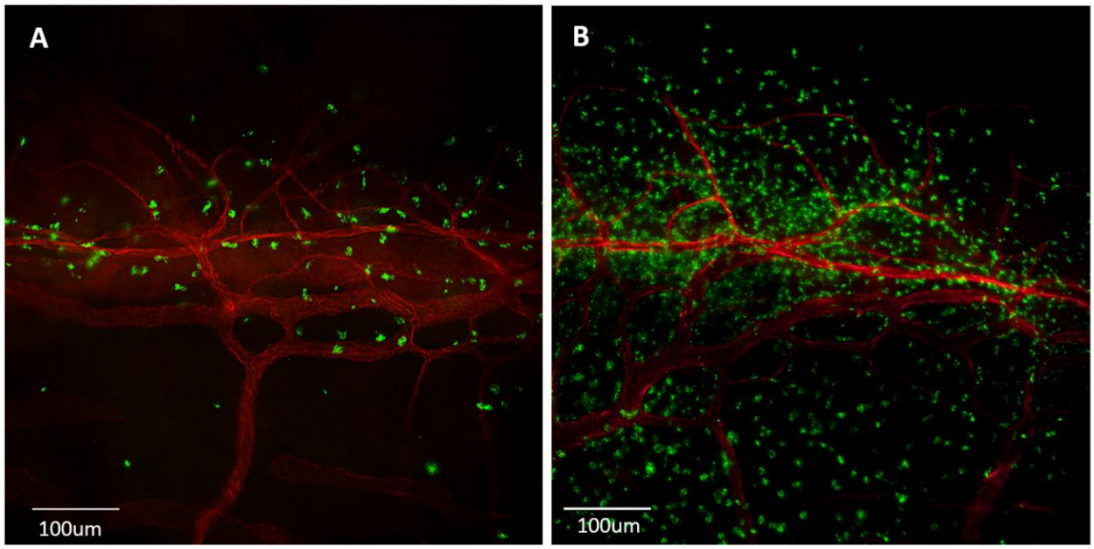

Figure 12. PMN extravasation at 12 PM and 9 PM in the superior quadrant of the mouse limbus.

PMN counts were variable as shown in this example where counts at 12 PM (left panel, 555/mm^2) were markedly lower than counts recorded at 9 PM (right panel, 1228/ mm^2).

An overall one-way ANOVA test was performed to compare means of PMN counts across eight time points (6 pm, 9 pm, 12 am, 3 am, 6 am, 9 am, 12 pm, 3 pm) with n=3 per time point. The data reveal no statistical difference between PMN counts for each time interval ($p=0.103$). Using the peak and nadir values recorded at 9 PM and 12 PM to estimate the effect size (mean difference in PMN counts), a power calculation was performed which suggested a sample size of n=5 would be necessary to detect this difference using a two-tailed t-test with $\alpha=0.05$ and 80% power.

To determine if PMN extravasation was similar in each quadrant (superior, inferior, nasal, temporal) we re-graphed the data. Four separate graphs were constructed to show PMN extravasation at eight separate time intervals (n=3) per 3h time interval (Figure 13). Qualitatively, PMN accumulation at the limbus of the temporal quadrant appeared lower than the other three quadrants.

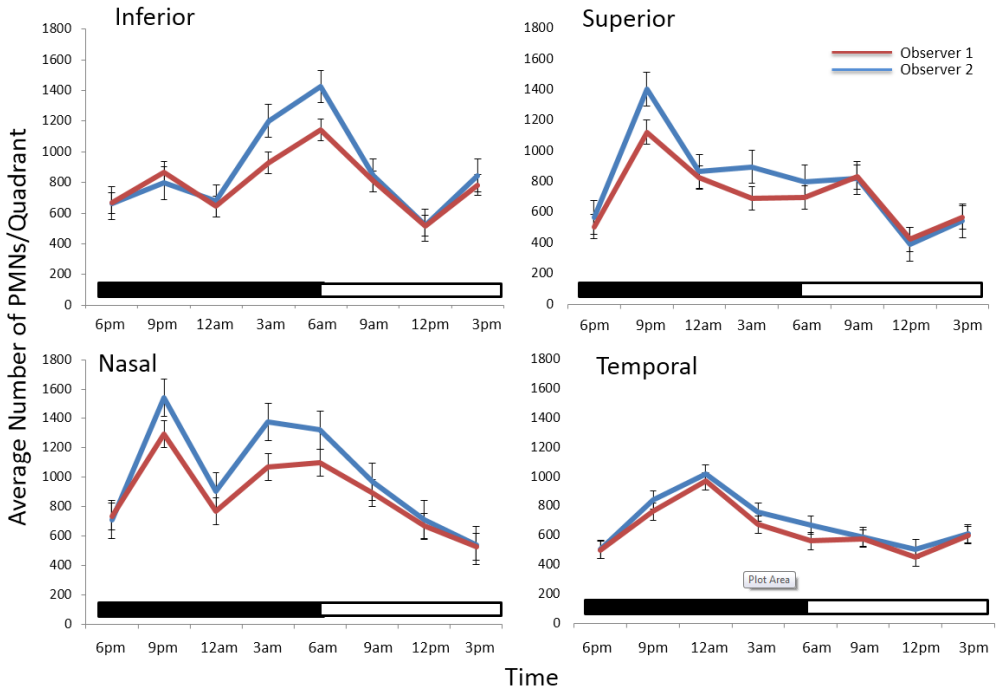

Figure 13: Extravasated PMNs by limbal regions at 8 time intervals

PMN extravasation counts displayed by 4 separate graphs to show anatomical regions (inferior, superior, nasal, and temporal). PMN counts per quadrant were evaluated with two observers: Observer 1, red; observer 2: blue.

Interobserver Data Analysis

A goodness-of-fit linear regression model testing the variability between counts of two observers revealed a coefficient of determination r^2= 0.8885, indicating that 88.85% of the data from each observer conform to a linear relationship. As shown by the testing, inter-observer calculations (Figure 14) revealed the independence of each observer. Therefore, for the remainder of the statistical tests in this thesis, PMN counts were sampled from Observer 1 for the purpose of including true counts, without combining to obtain mean values. Note: There was one observer for experiment 4.

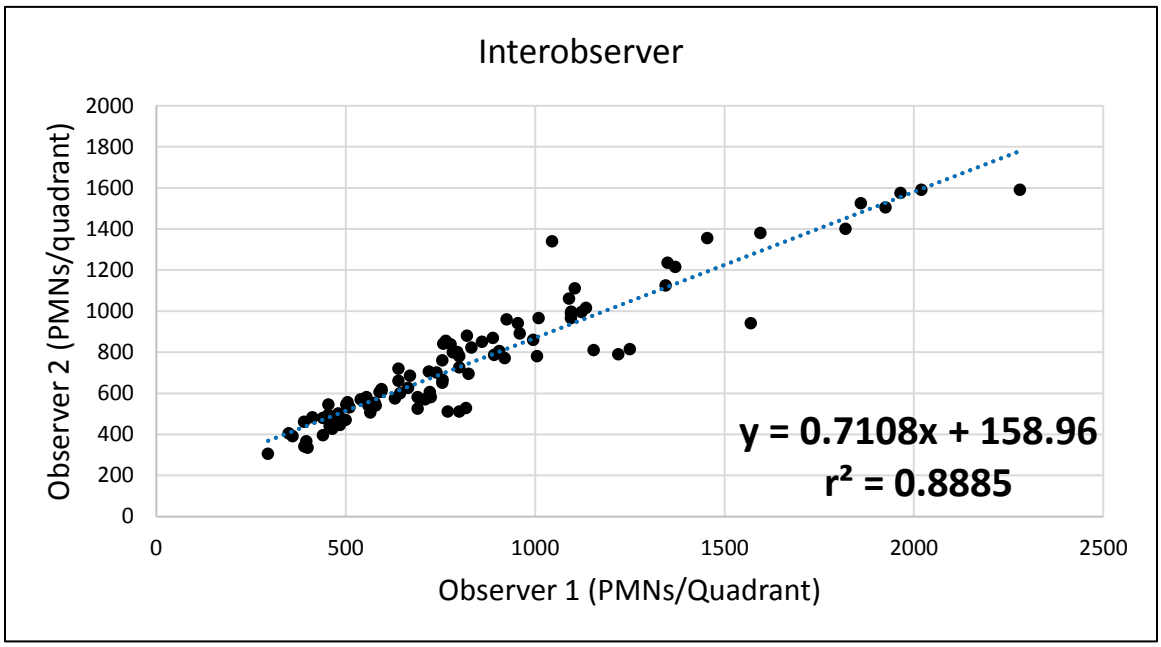

Figure 14. Interobserver data comparison for experiment 1

A goodness-of-fit linear regression model testing the variability between counts of two observers revealed a coefficient of determination r^2= 0.8885

PMN extravasation across four quadrants was not similar

Since PMN extravasation showed a non-similar distribution in the qualitative graphs (Figure 13), to determine if PMN extravasation across the 4 quadrants was quantitatively different, 8 separate chi-squared tests (one for each time point) were performed. For each of the 8 time-points, the chi-square tests showed the PMN counts were not evenly distributed among the quadrants ($p \leq .0001$), indicating the data were not sampled from a normal distribution (Tables 3 and 4). Significance was set at a p-value of ≤0.00625. To correct for multiple tests performed, the p-value was recalculated ($p=0.05/8$ where 8 is the number of tests). The results of the chi square test suggest there are regional (superior, nasal, inferior, temporal) differences in PMN extravasation.

Table 3. PMN Counts/quadrant across 8 time-intervals (n=3) in 24h period

	Superior	Nasal	Inferior	Temporal
6:00PM	500	720	640	590
6:00PM	440	595	560	360
6:00PM	755	820	795	565
9:00PM	1350	1965	1045	920
9:00PM	2280	2020	995	1095
9:00PM	580	640	350	510
12:00AM	454	458	465	758
12:00AM	1010	800	485	955
12:00AM	1135	1455	1090	1345
3:00AM	1220	1595	1155	710
3:00AM	725	1570	1820	1095
3:00AM	740	960	630	465
6:00AM	925	1005	1250	825
6:00AM	818	1860	1105	412
6:00AM	644	1096	1925	770
9:00AM	889	756	555	505
9:00AM	800	1370	1123	722
9:00AM	777	783	860	540
12:00PM	390	755	765	690
12:00PM	295	485	400	440
12:00PM	481	892	396	391
3:00 PM	502	464	906	595
3:00 PM	670	690	800	665
3:00 PM	456	455	832	577

The table shows counts for each time point (n=3 per time point) for each quadrant. Counts are expressed as PMN/quadrant. Values are given from observer 1 data. Data per time point are summed to get a grand total per quadrant for chi square analysis. These data are seen in table 4.

Table 4. Chi Square Test Results

Eight chi-square tests were performed for each 3h time interval. The corresponding chi-square values are displayed with p-values. P-value of ≤0.00625 was considered significant.

Time	Superior (total from 3 corneas)	Nasal	Inferior	Temporal	Expected value (25%)	Chi square value	p-value
6PM	1695	2135	1995	1515	1835	129.482	≤0.0001
9PM	4210	4625	2390	2525	3437.5	1145.258	≤0.0001
12AM	2599	2713	2040	3058	2602.5	205.998	≤0.0001
3AM	2685	4125	3605	2270	3171.25	676.853	≤0.0001
6AM	2387	3961	4280	2007	3158.75	1210.268	≤0.0001
9AM	2466	2909	2538	1767	2420	281.64	≤0.0001
12PM	1166	2132	1561	1521	1595	300.34	≤0.0001
3PM	1628	1609	2538	1837	1903	299.339	≤0.0001

Additionally, a relative frequency graph is shown here to visualize the differences in PMN extravasation in either superior, nasal, inferior, or temporal quadrants (Figure 15)

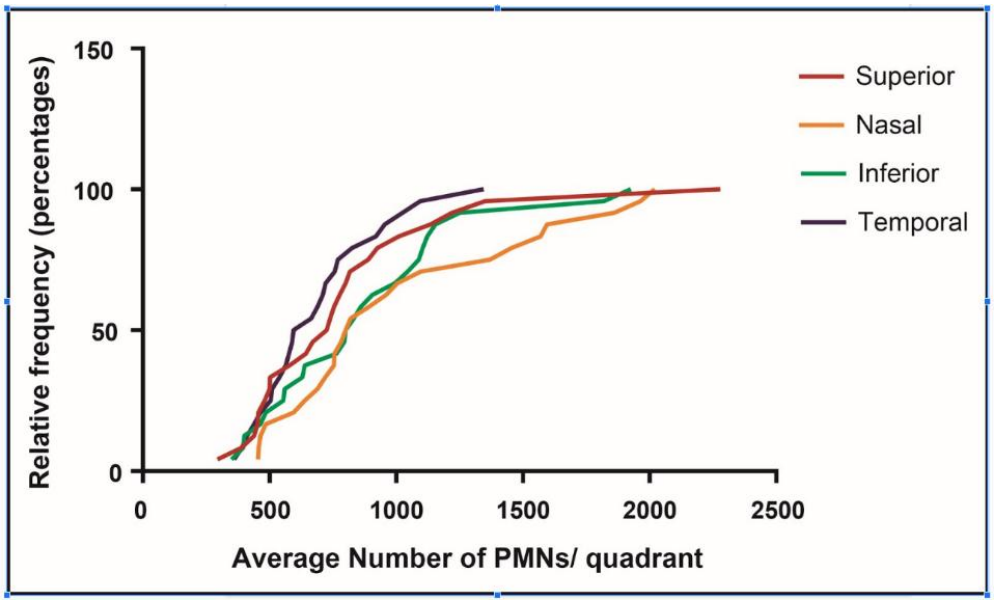

Figure 15. Extravasting PMNs for anatomical regions in the mouse limbus

A relative frequency graph anatomical regional (superior, nasal, inferior, temporal) PMN extravasation.

Because the temporal quadrant showed fewer PMN extravasation in both graphs and the chi square tests revealed a statistical difference in PMN extravasation, a post-hoc t-test was performed on the PMN counts for the nasal quadrant (1009 ± 364.09) and temporal quadrant (688 ± 177.38) and was found to be significant (p=0.04).

Experiments 2-4

For experiments 2, 3, and 4, for the purpose of simplifying the data with the focus on determining a difference between the peak and nadir PMN counts, we did not obtain data on separate quadrants, but analyzed PMN counts from the entire limbus. The extravascular PMN count for the entire limbus (all four quadrants) was determined without sub-dividing the data into quadrants. Thus, we did not electrocauterize the cornea prior to immunolabeling. We expressed the total PMNs per area of limbus in mm^2, rather than expressing counts per petal as was done in experiment 1, where the PMN distribution in each petal was counted. Only the areas that were counted were expressed in this calculation. This allows for any tissue that may have been damaged during the tissue processing to be non-contributory to the regions that were sampled. With this method, the amount of PMNs expressed per area normalizes the size variable.

Interobserver data was compared with a goodness of fit test and linear regression line. Again, the two observers showed agreement with each other in experiments 2 and 3 (r^2= 0.95 and r^2= 0.82, respectively). There was one observer for experiment 4. For this reason, statistical tests were performed with observer 1 data.

Experiment 2: PMN counts were similar in morning and evening after increase in sample size

A power calculation from experiment 1 showed a need for n=5 to achieve statistical significance if one were to compare only the peak and nadir. For this reason, a separate experiment was performed to determine whether there was an effect of sample size on the peak and nadir PMN flux in the uninjured mouse cornea. Mice were sacrificed at 9 PM and 12 PM to reflect the maximum and minimum counts found in experiment 1. A damaged corneal tissue during preparation of the slides disqualified one

of the samples from the 9 PM group. An unpaired t-test revealed no statistical difference between PMN counts for 9 PM (633 ±141.61) and 12 PM (623 ±234.83) in 11 corneas (p=0.94).

Experiment 3: PMN counts were similar in morning and evening after increase in sample size

Shortly after experiments 1 and 2 were completed, the CNRC vivarium underwent extensive renovations. Following the renovation and knowing that circadian cycles are sensitive to environmental cues, we repeated experiment 2 under different vivarium conditions. Using 5 mice per time-point, an unpaired t-test revealed no significant difference in PMN counts recorded at 9 PM (1274 ±297.50) and 12 PM (871 ±259.48) (p=0.052).

Experiment 4: Feeding mice a HFD for 10 days did not affect PMN extravasation

Given published evidence that metabolic syndrome can affect the circadian rhythm, we wanted to determine whether mice fed a HFD for 10 days (during which they develop signs of metabolic syndrome (Table 5)) affects PMN extravasation at the limbus.

Table 5. Metabolic syndrome parameters in mice fed a ND or HFD for 10 days

	ND	HFD
Body weight (gm)	27.3 ± 0.4	29.3 ± 0.7 *
eAT weight (gm)	0.44 ± 0.0	0.84 ± 0.09 ***
Fat mass (gm)	2.9 ± 0.25	5.85 ± 0.42 ***
Lean mass (gm)	24.26 ± 0.54	22.91 ± 0.55
Liver weight (gm)	1.67 ± 0.05	1.52 ± 0.09
Fasting Glucose (mg/dL)	192.1 ± 10.95	203.8 ± 10.77
Fasting Insulin (μg/ml)	0.82 ± 0.06	1.01 ± 0.048 *

*p<0.05, ***p<0.001, n=19

Additionally, these studies were performed in the winter (January) whereas studied described in experiments 1-3 were performed in the late spring (April-May). The winter time-point was of interest because diet-related induction of metabolic syndrome has been reported to be more evident in humans during the winter months[54]. In humans, metabolic syndrome parameters including insulin resistance, blood pressure, and blood glucose levels were higher during the winter months than the summer months[54].

Another modification performed in this experiment was the selection of the peak and nadir times. In experiments 1, 2, and 3, the peak and nadir were selected at 9 PM and 12 PM, respectively. Additional simultaneous studies in the laboratory being conducted by another researcher suggested the peak and nadir time-points may in fact be closer to 11 PM and 11 AM, respectively. Using these time-points, we found that a high fat diet does not affect PMN extravasation at the limbus. A two-way ANOVA (n=5) for each group (HFD or ND sampled at 11 PM or 11 AM) revealed no significant difference in PMN extravasation counts (p=0.29) (Figure 16). Additionally, an unpaired t-test revealed no significant difference in PMN counts between 11 PM (646 ±154.34) and 11 AM (609 ±141.81) in mice fed a ND (p=0.71) and an unpaired t-test revealed no

significant difference in PMN counts between 11 PM (908 ± 412.95) and 11 AM (635 ± 146.14) in mice fed a HFD (p=0.20).

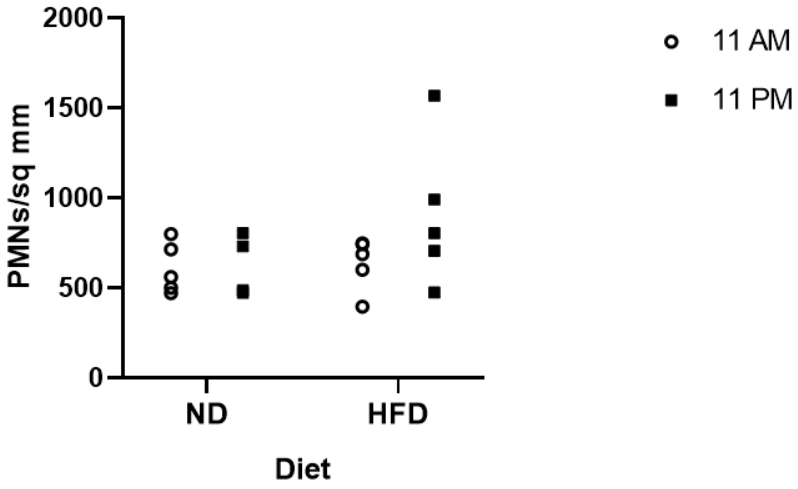

Figure 16. There was no apparent difference in PMN counts between 11 PM and 11 AM or between HFD and ND counts in 20 corneas

Two-way anova revealed no significant difference with a p-value of 0.29.

Pooling data from experiments 1-4 revealed a circadian pattern to PMN extravasation at the limbus

Because of the variability in PMN counts at the limbus, both between quadrants and overtime, we elected to pool the data from the four experiments to increase the sample size. We wished to determine, for future studies, if a larger sample size would be able to detect a circadian flux in PMN extravasation. We found that the evening PMN counts/mm^2 of limbus (9-11PM; 890.7± 359.9, n=18) was significantly greater (p=0.04) compared to the morning count (11AM- 12PM; 685.5 ± 220.3, n=19). We were unable to conduct a similar pooling of data for the HFD study as a HFD model was not used in experiments 1-3.

Chapter 4: Discussion

4.1 Aims for this thesis

4.1.2 HFD feeding revealed non-confirmative conclusions on PMN circadian flux

4.1.3 The need for a larger sample size when analyzing PMN circadian flux

4.2. Our results showed a modest increase in PMN counts

4.3 Significance of this study

4.3.1 Why are PMNs present in the uninjured limbus?

4.3.2 PMN extravasation at the limbus is not uniform across all quadrants

4.3.3 Influx of PMNs during non-inflammatory conditions

4.4 Clinical implications

4.4.1 Clinical relevance of studying circadian rhythm in the mouse model

4.4.2 Why do we study circadian rhythm?

4.5 General conclusions and future directions

4.5.1 Strengths of this study

4.5.2 Limitations of this study

4.5.3 Future directions

Aims for this thesis:

Specific Aim 1: To determine if there is a circadian pattern of PMN extravasation at the uninjured mouse limbus

Specific Aim 2: To determine if PMN extravasation at the uninjured limbus is disturbed by environmental influences of diet induced obesity caused by a high fat diet.

The purpose of this thesis was to determine if there is a circadian pattern of PMN infiltration. This study showed that PMN extravasation at the uninjured mouse limbus follows a circadian pattern where PMN extravasation increases moderately during the evening. Extravasation in the uninjured cornea is non-uniform and lower in the temporal quadrant. PMN counts showed a peak (890.7± 359.9, n=18) between 9-11 PM and a nadir 685.5 ± 220.3, n=19 between 11 AM-12 PM (p=0.04). This was only evident after pooling the data to increase sample size (n=18-19).

HFD feeding revealed non-confirmative conclusions on PMN circadian flux

In experiment 4, we tested whether a HFD has an effect on PMN extravasation. We found no significant difference in PMN extravasation in mice fed a ND and HFD (p=0.29). Additionally, there was no significant difference in PMN counts between 11 PM (646 ±154.34) and 11 AM (609 ±141.81) in mice fed a ND (p=0.71) and no significant difference in PMN counts between 11 PM (908 ± 412.95) and 11 AM (635 ± 146.14) in mice fed a HFD (p=0.20). Pooling was not possible for the HFD study and for this reason, no firm conclusions can be drawn regarding the effects of a HFD on PMN extravasation at the limbus because the study was underpowered by virtue of its smaller sample size (n=5).

The need for a larger sample size when analyzing PMN circadian flux

For experiments 1-4, each individual experiment revealed no significant difference in PMN counts between evening (peak) and morning (nadir) time points. The finding of a circadian PMN flux was only evident after pooling of the data to increase sample size (n=18-19). The need for larger sample sizes is consistent in studies by Frenette *et al.* who observed PMN circadian rhythms in other tissues. It would behoove future studies involving circadian rhythms, at least for PMN extravasation, to have a larger sample size (n~20).

Our results showed a modest increase in PMN counts

PMN extravasation at the limbus has been reported in the literature and was found to show an approximately 4-fold increase during the evening[55]. Two factors may explain the more modest increase (1.4-fold) reported in this thesis. First, the limbal PMN counts made by Li and colleagues were made from female mice. It has been shown that there are obvious differences in corneal wound healing between male and female mice[56]. Following a central epithelial abrasion, the wounds of female mice closed 6 hours earlier than that of males[56]. Furthermore, female mice exhibited a 24-hour delay in peak PMN emigration to the site of injury[56]. Although this phenomenon was observed in an acute inflammatory model, given the sex differences in PMN infiltration, sampling from male mice done in this thesis would likely give differing results.

The second plausible reason for the more modest increase in PMN counts in this thesis is that there were significant differences in the methods used to determine PMN counts. The published study by Li and colleagues estimated PMN infiltration by taking counts from only one-third of the available limbal area[55]. Given PMN accumulation at the limbus is non-uniform and varies between quadrants, sampling only one-third of the limbal

area is less likely to provide accurate estimates when compared to counting all the PMNs with the entire limbus of the cornea as was done in this thesis. Our data indicate PMN distribution is not homogeneous (see Results) and varies showing temporal quadrant showing lowest amount of PMN extravasation. Only by counting the total PMNs in the entire cornea is one able to obtain accurate counts.

Significance of this study

Why are PMNs present in uninjured limbus?

It has been shown that PMNs are present in the uninjured tissues like the spleen, bone marrow, and liver[39]. These "aged" PMNs as discussed earlier, participate in specialized functions like moderating innate immunity, promoting angiogenesis, and metabolic regulation for peripheral organs. For example, aged PMN clearance functions in the bone marrow by regulation of the hematopoietic niche, the primary controller for all hematopoietic stem and progenitor cells (HSPCs)[39]. PMN clearance regulates HSPCs by mediating the expression of cytokine granulocyte-colony stimulating factor (G-CSF) within the hematopoietic niche[57]. PMNs are also shown to exhibit a circadian pattern in these tissues, including the bone marrow and skeletal muscle tissue. Frenette *et al*. observed an approximately 2-fold increase in PMNs within the bone marrow in the evening, peaking at Z13[51]. This PMN increase in the uninjured tissue coincided with HSC, indicating that PMNs play a role in HSC recruitment to the bone marrow. Since PMNs are present in circadian patterns in peripheral tissues, it was reasonable to hypothesize. This thesis showed that there is PMN extravasation in the uninjured cornea, and this PMN extravasation exhibits a circadian pattern. However, the reason for PMN infiltration into the cornea and other peripheral tissues under normal physiologic

condition is unclear. As previously discussed, in a mouse model of a corneal epithelial abrasion along with the removal of the subbasal nerve plexus, the recruitment of PMNs along with platelets are evident via a γδ T-cell-dependent inflammatory cascade[47]. Furthermore, IL-17, a chemoattractant for PMNs to migrate to the site of injury is present, and infiltrating PMNs (and platelets) bring VEGF into the cornea, which promotes efficient nerve regeneration[47].

Given that in inflammation, infiltrating PMNs are a rich source of VEGF-A, the possibility is raised that PMN extravasation in the uninjured cornea may play an important role in corneal nerve homeostasis. The increased accumulation of PMNs in the evening may provide a necessary boost in VEGF-A release that sustains nerve growth and extension towards the central cornea. This suggestion would gain support if we were able to show that a HFD blunts the circadian flux because the HFD clearly reduces corneal nerve sensitivity and density. However, in the current study, we only had 5 mice in a group for the HFD and, as we have shown in this thesis, a minimum number of 20 mice per group is needed to power the statistical analysis. Repeating the HFD study (experiment 4) with a larger group of mice would determine if a reduction in PMNs occurs as a result of the HFD, establishing a possible link between PMNs and nerve homeostasis.

Another explanation for PMN extravasation at the limbus is suggested by studies of hematopoietic stem cells (HSCs) and lymphocytes which exhibit a steady infiltration within other tissues and serve a protective role within the immune system[48]. Within the bone marrow, the recirculation of HSPCs are necessary for providing robust responses to distress signals from the local environment[48]. This homing of recirculating HSPCs is understood to be necessary for maintenance of hematopoietic homeostasis within bone

marrow cavities[58]. Given that PMNs also exist in peripheral uninjured tissues including the bone marrow, it would seem reasonable that PMNs may be similarly providing an imnunosurveillance functionality by being present in uninjured tissues like the corneal limbus, allowing them to respond in a rapid fashion under abrupt insult or injury.

PMN extravasation at the limbus is not uniform in all quadrants

In experiment 1, we addressed the notion that PMN extravasation may not be equally distributed across regional anatomical quadrants (superior, nasal, inferior, temporal). Chen *et al*. discovered in 2010 that the distribution of blood vessels and lymphatic tissues in commonly studied mouse models, BALB/c and C57Bl/6 mice, is unevenly distributed under normal conditions[59]. Their studies revealed that both corneal and lymphatic vessels showed a nasal-dominant pattern of distribution. A similar phenomenon of differential distribution of vasculature occurs in ocular tissues like the retina[60]. For example, there is a predominance for arterial-venular crossings to occur in the superotemporal quadrant of the retina, which is why branch retinal vein occlusions have a predilection to occur in the superotemporal quadrant. These corneal and retinal observations raised the possibility that PMN extravasation at the limbus was unlikely to show an even distribution. Graphically, it appeared that PMN extravasation was lowest in the temporal quadrant and highest in the nasal quadrant. This was confirmed using Chi squared statistics where actual PMN counts failed to follow the predicted uniform quadrant value (i.e., total counts/4 to produce an expected uniform distribution). Additional post-hoc analysis of the temporal region compared with the nasal region using an unpaired student t-test revealed far fewer PMNs accumulate in the temporal region over a 24h period compared to the other three quadrants. It is worth noting that gross observation of the limbal vasculature revealed no obvious anatomical differences

(number of capillary loops, vessel width, or overall relative complexity of the vasculature across the four examined quadrants (superior, nasal, inferior, temporal). That being said, it remains to be determined why the temporal limbal vasculature supports less PMN extravasation. It would be of interest to know if PMN extravasation during inflammation is similarly low in the temporal quadrant following a central epithelial abrasion. Indeed, Chen *et al*. reported the vessels respond differently during corneal inflammation, characterized by lymphangiogenesis and hemangiogenesis[59]. It was discovered that during inflammation, blood vessels lost their typical nasal dominance pattern, while lymphatic vessels maintained nasal dominance. Whether PMN extravasation follows an analogous pattern for regional distribution under inflammatory conditions is unknown.

Influx of PMNs during non-inflammatory conditions

While it is clear circadian PMN extravasation into uninjured tissues is a relatively common occurrence[39,51], the process by which PMNs exit the blood vessel is unclear. The process by which differentiated PMNs extravasate from an inflamed endothelial vessel is well understood (see Introduction). However, in the absence of overt inflammation or injury, the process of exiting the blood vessel is different and poorly understood. In inflamed tissues, PMNs must first tether and then roll along the inflamed endothelium prior to arresting and transmigrating. In the systemic circulation, this occurs primarily in post-capillary venules, the diameter of which exceed that of the PMN. The selectin family of adhesion molecules mediates the initial capture (tethering) of the PMN and the subsequent rolling along the inflamed endothelial surface. Increased ICAM-1 expression on the endothelium enables PMN arrest and transmigration. However, in uninflamed tissues, it seems an increase in ICAM-1 is sufficient for PMN

extravasation[39,61]. Frenette *et al.* showed that PMN circadian rhythm in peripheral tissues is mediated by a tissue-specific circadian rhythm of endothelial adhesion molecule expression. PMN recruitment coincided with the oscillations in ICAM-1 protein expression and V-CAM-1 in the cremaster muscle and bone marrow, respectively[51]. Why selectins are not needed in this mechanism is unclear, but with respect to the limbal vasculature, from face-to-face discussion with Dr. Burns, it is possible to imagine that elevated ICAM-1 expression in the capillary loops would be sufficient for PMN arrest and transmigration because the small diameter of these vessels forces the PMN to change shape and squeeze through the capillary lumen and in so doing come into contact with ICAM-1. Using this mechanism, PMN tethering and rolling would be unnecessary, hence PMN extravasation occurring in the absence of inflammatory mediators like platelet and erythrocytes. This postulation may be prospective when one examines the images of the PMN extravasation taken from results from experiment 1 (Figure17). PMN extravasation is shown at 12 PM and 9 PM. A line demarcating a clinical boundary between the post-capillary venules and the capillary loops is shown to compare PMN extravasation proximal to the capillary loops (above the line) and at the post-capillary venules (below the line). At both nadir and peak time points, morning (12 PM) and evening (9 PM), PMN counts appear to be higher at regions near the capillary loops, indicating PMN extravasation at the capillary loops could be a consistent occurrence for PMN extravasation, regardless of time.

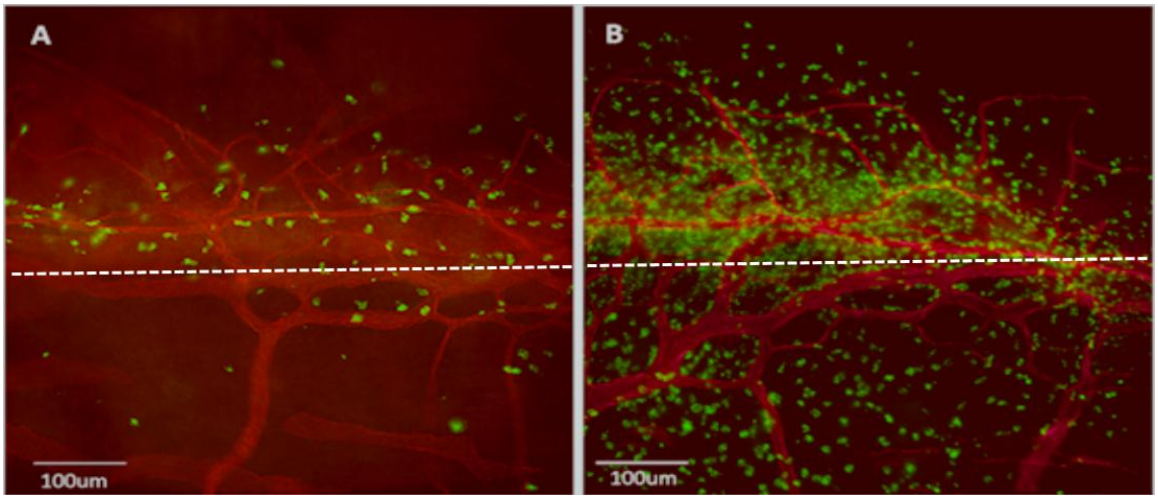

Figure 17. PMN extravasation appears to favor capillary loops region at both 12 PM and 9 PM

Images of PMN extravasation taken from results from experiment 1, showing PMN extravasation at (panel A) 12 PM and (panel B) 9 PM. The white dashed line indicates a clinical boundary between the post-capillary venules and the capillary loops. More PMNs are seen over the small diameter capillary loops than over the larger venules.

It would be of interest in future studies to explore the difference in PMN extravasation within the regions of post-capillary venules and capillary loops. Figure 18 depicts a representation of PMN extravasation during inflammation with the presence of platelets and erythrocytes via the post-capillary venules compared with the proposed PMN extravasation during non-inflammation via capillary loops in the absence of platelets, erythrocytes and other inflammatory modulators (not depicted).

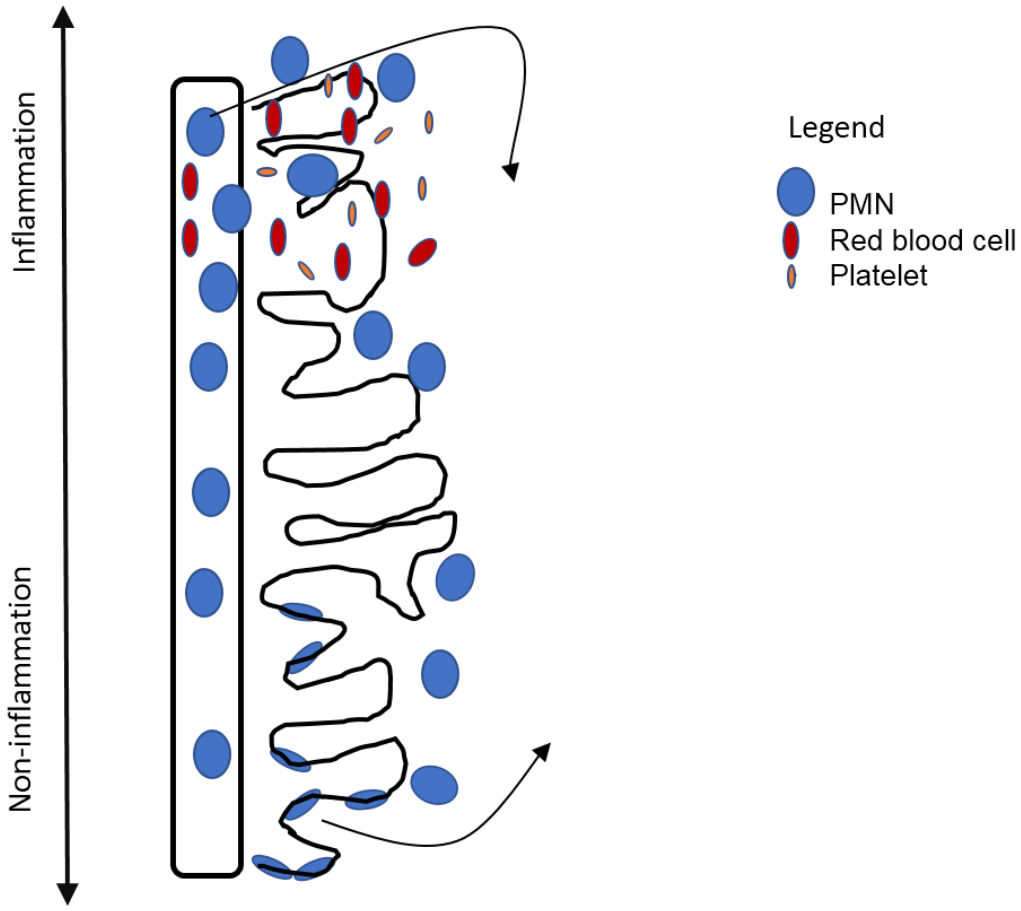

Figure 18. PMN extravasation in the limbus during inflammation and (proposed mechanism) during non-inflammation

Schema displaying PMN extravasation in the limbus under two conditions: inflammation (top) and non-inflammation (below). In systemic circulation (top), where the PMN tethers along inflamed endothelial vessel, arrests, and transmigrates with the presence of inflammatory mediators like platelets and erythrocytes (red blood cells). On the other hand, PMN extravasation in the absence of inflammation, it is proposed that the PMN exits through the smaller diameter capillary loops, where it changes shape to squeeze out of the vessel, without the presence of red blood cells or platelets.

PMN migration in the lung during inflammation shows a similar mechanism to this proposed mechanism. Rather than migrating out of the post-capillary venules like in most systemic circulation, the PMNs extravasate out of capillaries[62]. The capillary bed in the lung contains a large interconnected network of short capillaries approximately 7.5 µm in diameter. The small diameter of the capillaries, relative to the PMN (6.8 µm) causes the PMN slows down in its path of migration, allowing the cell to be in close proximity with the endothelium[62]. Although this is occurring during inflammation and in the lung tissue, it could be possible PMN extravasation in the uninjured limbus is similar. Perhaps when the PMN slows down, it is coming into contact with ICAM-1 expressed on the endothelium, aiding in its extravasation. Future studies should consider determining if ICAM-1 is selectively upregulated in the capillary loops. Moreover, blocking antibodies directed against ICAM-1 should reduce PMN peak counts in the evening whereas antibodies against the selectins would be expected to have little effect. In fact, Frenette *et al*. observed in an ICAM-1 knockout presentation in LPS-induced septic shock, the circadian flux of PMN extravasation was blunted[51].

PMNs show a normal influx within the tear film in the closed-eye environment. Every day, during sleep, there is a normal change in tear composition including the increases in metalloproteinases and cytokines correlating to increases in leukocyte recruitment to the tear film[63]. Following 8 hours of sleep, the concentration of inflammatory cells at the ocular surface is approximately 3×10^7 cells/mL, with PMNs accounting for 58% of the total cell collection. Based on receptor expression and oxidative products, the behavior of the tear-film PMNs within a closed-eye system was significantly different from that of blood-isolated PMNs. Tear-film PMNs did not respond to inflammatory stimuli as blood-isolated PMNs did. The evidence supports the concept

that tear-film PMNs are anti-inflammatory as evidenced by the presence of lactoferrin and other anti-inflammatory mediators at the ocular surface. There is evidence of phenotypical and functional changes in uninjured tissues in the absence of inflammation, relating to the differentiated purpose of PMNs in innate and adaptive immunity[63,42]. For example, fresh and aged PMNs express different chemokines for the purpose of being cleared into different tissues to perform specialized functions, as discussed earlier (see Introduction). Much more needs to be uncovered on this concept and understanding the phenotypical change and role of PMNs in non-inflammatory conditions warrants further study.

The increasing epidemic of the ocular surface disorder, dry eye disease, has been intensely studied and now understood to be an ocular surface inflammation characterized by increased stress of chemokines, cytokines, and metalloproteinases (MMPs)[64]. The inflammatory cycles are prolonged by the activation of T-cells and adhesion molecules ICAM-1 and leukocyte, LFA-1 expression are implicated to follow. Indeed, newer drug therapies which are designed to disrupt the inflammatory cascade, are designed to target the coupling of LFA-1 and ICAM-1[65]. Due to the viscous nature of the inflammatory cycle and the complexity of diagnosis and treatment, this multifactorial disease is still not well understood and is under ongoing research[64,65,66]. While we are aware that the ocular surface including the cornea is under a chronic, localized inflammation, it is unknown whether this chronic inflammation could be a stimulating factor for recruitment of PMNs into the limbus.

Clinical Implications

The clinical relevance of studying circadian rhythm in the mouse model

Mice are a particularly useful model for studying circadian rhythmicity due to the ease of genetic manipulation, thus identifying molecular contributors to rhythmicity. Furthermore, their small size allows for monitoring movement or activity in their caged environment with relative ease. Light is one of the most powerful forms of entrainment of the circadian rhythm. All mammals, including humans are entrained by photopic cues in the environment, allowing the organism to synchronize to a biological clock. Similar to other mammals, including humans, mice typically have a circadian rhythm slightly shorter than a 24-hour period[67]. Although mice are nocturnal, they are still entrained the same way as humans are—by an external cue, predominantly light[67]. Researchers can use a light/dark cycle to an advantage in studying the behavior of circadian rhythm. Manipulating the light phase in mice to allows the opportunity to study the phototopic entrainment in humans as well as the influence of environmental factors such as a HFD on behaviors of the circadian rhythm.

Why do we study circadian rhythm?

All organisms are tethered by a biological clock which influences multiple circadian rhythms including sleep/wake cycles, hormonal release cycles, digestion, and many other physical and behavioral functions. The biological clock is an endogenous clock that syncs the organism to the external clock like the 24-hour light/dark cycle in humans and rodents. All organisms have multiple circadian rhythms which are synchronized by a primary clock, the suprachiasmatic nucleus (SCN)[68]. Environmental signals, primarily light, sends signals to the SCN and can affect our internal circadian rhythms by turning on or off the expression of genes, resulting in different behavior and

physical changes. For example, a decrease in light triggers the SCN to allow the release of melatonin, a sleep hormone[68]. Because external cues heavily control our internal circadian rhythms, any change in pace of the biological clock or shifting of the clock, made by instances like an altered sleep-wake cycle, will cause a disruption in the circadian rhythm[69,70].

Common examples of a disruption to the sleep-wake cycles controlled by light phases and dark phases are individuals performing shift work or travelers passing through different time zones and experiencing jetlag[70]. Many of these circadian disturbances can lead to numerous chronic illnesses like sleep disorders, mental health issues, digestive disorders[69]. Societal changes in the recent years have led to busier lives, work shifts extending into overnight hours, and stress causing insomnia, allowing one to easily fall into the trap of a disrupted sleep-wake cycle[70]. In fact, the Bureau of Labor Statistics reported approximately 15% of the workforce in the US is made up of shift workers. Additionally, an increase of approximately 831 million airbound travelers globally was reported from the year 2011 to 2016. Chronic abnormalities in circadian rhythms that these individuals experience can become detrimental. A meta-analysis found a positive correlation between increased years of shift work to risk and the likelihood of developing breast cancer in females[71]. Additionally, gastrointestinal disorders like peptic ulcer disease have been linked to shift workers[72]. A cohort study also found links to cancer in individuals experiencing long-term jetlag[73]. Because of this widespread of shift work and jet lag in society, circadian study and the negative impacts of disrupted circadian has become increasingly important.

It has also been noticed that dietary changes and obesity have been known to disturb circadian rhythms. Disruptions in sleep cycles are correlated to metabolic

changes that put an individual at higher risk for type 2 diabetes and metabolic syndrome. Several metabolic factors like glucocorticoids and *Rev-erb alpha* exhibit a circadian pattern in humans and rodents. The increasing epidemic of type 2 diabetes and obesity permits further study as to how HFD and metabolic syndrome affect the circadian rhythm. The aforementioned studies in our lab show a HFD leads to changes in the cornea, such as a decrease in corneal density and sensitivity (Burns et al., unpublished data, 2019, see Introduction). Additionally, as discussed earlier, a feeding of a HFD has shown to blunt the circadian expression of a clock gene, *Rev-erb alpha* within the mouse cornea (see Introduction). It would be plausible to presume that since HFD disrupts circadian expression of genes, it would similarly alter PMN infiltration at the limbus. In this thesis, by virtue of a small sample size, experiment 4 was unable to obtain firm conclusions on whether a HFD affects the circadian flux of PMN extravasation. Therefore, further investigations on HFD and circadian rhythms should warrant larger sample sizes. One would highly suspect that HFD and obesity play a large role in disrupting circadian rhythms of PMN extravasation.

Studying how the biological clock is influenced by external factors like metabolic syndrome enables us to understand circadian rhythm in all organs and tissues of the body, including the cornea. Given that in inflammation, infiltrating PMNs are a rich source of VEGF-A[47], the increased accumulation of PMNs in the evening, as evident in this thesis, may provide a necessary boost in VEGF-A release that sustains nerve homeostasis. This suggestion would gain support if future studies show that a HFD blunts the circadian flux because the HFD clearly reduces corneal nerve sensitivity and density. Importantly, 70% of diabetics exhibit keratopathy and, in the mouse, loss of corneal sensitivity seems to precede the development of insulin resistance and

hyperglycemia (unpublished data). If we establish a link between HFD and corneal homeostasis, it would provide future implications for studies regarding early diagnostic tools for keratopathy in diabetic and or obese patients.

General Conclusions and Future Directions

The data in this thesis collectively demonstrates that there is a significant difference in PMN extravasation between morning and evening times in uninjured corneas of mice fed a ND. The data also show that large sample sizes are necessary to reveal a circadian pattern, and in our study, this required a pooling of the data. This finding is consistent with other studies in the literature showing large numbers of mice are needed to document the circadian PMN rhythms[74,61]. We were unable to comment about HFD by virtue of a small sample size.

Strengths in our study

Anatomical regional preference

We demonstrated that there was no preference for anatomical regions in PMN infiltration. We found no preference for anatomical regional (superior, inferior, nasal, temporal) PMN infiltration at the uninjured mouse limbus. A study in murine corneal anatomy shows that lymphatic and blood vessels do not show an even distribution in the limbus. Lymphatics and blood vessels are more developed on the nasal side in the murine cornea. The nasal-dominant distribution of vessels provides the implication that PMN infiltration may be also be preferential to the nasal side[59].

High fat diet mouse model

For a HFD mouse model in experiment 4, the duration of a 10-day HFD induced elements of metabolic syndrome were detectable when mice were evaluated after the tenth day of initiation of the diet (unpublished data, Smith and Burns, 2019). The mice exhibited significant increases in body weight, intra-abdominal epididymal fat pad weight, and a 2-fold increase in fat mass (see Results, Table). A strength in our study was using only male mice, because female mice do not exhibit the negative consequences from consumption of a HFD as male mice do[53]. In a study, after a 14-week HFD, although female mice display similar weight gain as male mice, they did not develop low-grade systemic inflammation as well as other HFD parameters that the male mice developed[53].

Limitations of this study and ways to improve future studies:

1. This study was limited by the lack of a "circadian box." The frequent disturbances within the housing conditions such as feeding and handling could have caused a disruption in the regular circadian cycles of the mice. Future circadian studies would benefit from using circadian chambers.
2. This study was limited on sample size. Each separate experiment demonstrated a non-significant result in the difference between PMN extravasation in the evening versus morning. However, with a larger sample size, when all samples were combined, there was a significant difference between evening and morning PMN extravasation. Future studies will have to consider using more mice (e.g., n=20 per group).

Future Directions

Critical housing conditions

Minimal disruption to the housing conditions are essential when performing circadian phenotyping[67]. Minor interferences such as cage changing or water and food swapping "can affect the circadian response to photoperiod manipulation"[67]. Shipping mice can also affect their circadian patterns. Future studies can minimize these disturbances using a circadian chamber.

Studying vasculature differences across anatomical region (superior, nasal, inferior, temporal)

The data in this thesis suggested a regional preference for PMN extravasation at the limbus with the least preference being the temporal quadrant. A possible motivating study could be to determine if there is a quantifiable difference in vasculature complexity in the uninjured mouse limbus. While previous studies discovered a nasal-dominance pattern of blood vessel and lymphatic distribution, the methodology of determining vasculature dominance was restricted to two quadrants. Suture markers were placed at 3 o'clock and 9 o'clock, essentially separating the cornea into nasal and temporal halves. It would be interesting to document vascular organization differences across the four quadrants under normal physiologic conditions, absent of overt inflammation. The study could incorporate factors such as vessel diameter and amount of capillary loops. Additionally, we would be encouraged to see whether vessel distribution changes in a HFD.

Effect of HFD on photoentrainment signals

Photoentrainment signals are sent to the two main targets of the circadian regulator system: the SCN of the hypothalamus and the intergeniculate leaflet of the thalamus (IGL)[75]. The SCN is considered to function as the "master clock," where light activates neurons containing melanopsin in the retina sending the signals to the SCN[67]. It has been shown that light cues perceived through the visual pathway via the rods and cones and cues from intrinsically photosensitive retinal ganglion cells (ipRGCs) collectively provide entrainment information for the circadian rhythm. It would be interesting to study whether a systemic inflammation caused by a HFD causes a disruption to either of these mechanisms of transmission of entraining information that could in turn affect the circadian flux of PMN infiltration.

In vivo studies performed with HRT

In vivo confocal microscopy using the Heidelberg Retinal Tomographer III with the Rostock Corneal Module (HRT-RCM) provides live *in vivo* leukocyte cell motility image recordings[76]. This process is performed without surgical intervention, and therefore in uninjured, "normal" settings"[77]. Perhaps *in vivo* studies may provide more benefit in tracking PMN extravasation in circadian studies. With the live tracking of cellular trafficking we could track PMN extravasation with a second-by-second analysis. We could expect to obtain more insight on the exact timing of the peak and nadir of PMN extravasation. Furthermore, we would be able to determine if PMN extravasation per quadrant is different.

Bibliography (or References)

1. Eghrari AO, Riazuddin SA, Gottsch JD. Overview of the Cornea.*Prog Mol Biol Tran Sci*; 2015;134 (1): 7-23.
2. Bergmanson JPG. *Clinical Ocular Anatomy and Physiology*. 23rd ed. (Bergmanson JPG, Hemmati R, eds.). Houston, TX: Texas Eye Research and Technology Center; 2016;71-137.
3. Hanna C, Bicknell DS, O'brien JE. Cell Turnover in the Adult Human Eye. *Arch Ophthalmol*. 1961;65(5):695-698.
4. Hanna C. Cell Production and Migration in the Epithelial Layer of the Cornea. *Arch Ophthalmol.*1960; 64(5):536-539.
5. Torricelli AAM, Singh V, Santhiago MR, Wilson SE. The corneal epithelial basement membrane: Structure, function, and disease. *Investig Ophthalmol Vis Sci*. 2013;54(9):6390-6400.
6. Alarcon I, Kwan L, Yu C, Evans DJ, Fleiszig SMJ. Role of the corneal epithelial basement membrane in ocular defense against Pseudomonas aeruginosa. *Infect Immun*. 2009;77(8):3264-3271.
7. Mathew JH, Bergmanson JPG, Doughty MJ. Fine structure of the interface between the anterior limiting lamina and the anterior stromal fibrils of the human cornea. *Investig Ophthalmol Vis Sci*. 2008;49(9):3914-3918.
8. Komai Y, Ushiki T. The three-dimensional organization of collagen fibrils in the human cornea and sclera. *Investig Ophthalmol Vis Sci*. 1991;32(8):2244-2258.
9. DelMonte DW, Kim T. Anatomy and physiology of the cornea. *J Cataract Refract Surg*. 2011;37(3):588-598.
10. Matthyssen S, Van den Bogerd B, Dhubhghaill SN, Koppen C, Zakaria N. Corneal regeneration: A review of stromal replacements. *Acta Biomater*. 2018;69:31-41.
11. Y.M. M. Collagens and proteoglycans of the corneal extracellular matrix. *Brazilian J Med Biol Res*. 2003;36(8):1037-1046.
12. Hanlon SD, Behzad AR, Sakaic LY, Burns AR. Corneal Stroma Microfibrils Samuel. *Exp Eye Res*.2016; 0:198-207.
13. Hassell J, Birk D. The molecular basis of corneal transparency. *Exp Eye Res*. 2010;91(3):326-335.
14. Maurice DM. the Structure and Transparency of the Cornea. *J Physiol*. 1956;36:263-286.
15. Doughty MJ, Bergmanson JPG. Collagen fibril characteristics at the corneo-scleral boundary and rabbit corneal stromal swelling. *Clin Exp Optom*. 2004;87(2):81-92.
16. Bergmanson JPG, Horne J, Doughty MJ, Garcia M, Gondo M. Assessment of the number of lamellae in the central region of the normal human corneal stroma at the resolution of the transmission electron microscope. *Eye Contact Lens*. 2005;31(6):281-287.
17. Meek KM, Leonard DW, Connon CJ, Dennis S, Khan S. Transparency, swelling and scarring in the corneal stroma. *Eye*. 2003;17(8):927-936.
18. Bergmanson JPG, Sheldon TM, Goosey JD. Fuchs' endothelial dystrophy: A fresh look at an aging disease. *Ophthalmic Physiol Opt*. 1999;19(3):210-222.

19. Lampugnanf MG, Farmacologiche R, Negri M. Intercellular Junctions in the Endothelium and the Control of Vascular Permeability. *Ann N Y Acad Sci*. 1997;811:36-44.
20. Bourne WM. Cellular changes in transplanted human corneas. *Cornea*. 2001;20(6):560-569.
21. Shaheen BS, Bakir M, Jain S. Corneal nerves in health and disease. *Surv Ophthalmol*. 2014;59(3):263-285.
22. Wang S, Ghezzi CE, Gomes R, Pollard RE, Funderburgh JL, Kaplan DL. In vitro 3D corneal tissue model with epithelium, stroma, and innervation. *Biomaterials*. 2017;112:1-9.
23. De Felipe C, Gonzalez GG, Gallar J, Belmonte C. Quantification and immunocytochemical characteristics of trigeminal ganglion neurons projecting to the cornea: Effect of corneal wounding. *Eur J Pain*. 1999;3(1):31-39.
24. Müller LJ, Marfurt CF, Kruse F, Tervo TMT. Corneal nerves: Structure, contents and function. *Exp Eye Res*. 2003;76(5):521-542.
25. Michael Van Buskirk E. The Anatomy of the Limbus. *Eye*. 1989;3:101-108.
26. Goldberg MF. Limbal Palisade of Vogt. *Trans Am Ophthalmol Soc*. 2005;80:155-171.
27. Marando CM, Park CY, Liao JA, Lee JK, Chuck RS. Revisiting the cornea and trabecular meshwork junction with 2-photon excitation fluorescence microscopy. *Cornea*. 2017;36(6):704-711.
28. Al-Mahmood AM, Al-Swailem SA, Edward DP. Glaucoma and Corneal Transplant Procedures. *J Ophthalmol*. 2012;2012:1-9.
29. Papas EB. The limbal vasculature. *Contact Lens Anterior Eye*. 2003;26(2):71-76.
30. Hanlon SD, Smith CW, Sauter MN, Burns AR. Integrin-dependent Neutrophil Migration in the Injured Mouse Cornea. *Exp Eye Res*. 2014; 120:61-70.
31. Burns AR, Li Z, Smith CW. Neutrophil Migration in the Wounded Cornea: The Role of the Keratocyte. *Ocul Surf*. 2005;3(4):173-176.
32. Feneck EM, Lewis PN, Ralphs J, Meek KM. A comparative study of the elastic fibre system within the mouse and human cornea. *Exp Eye Res*. 2018;177:35-44.
33. Van der Merwe EL, Kidson SH. The three-dimensional organisation of the post-trabecular aqueous outflow pathway and limbal vasculature in the mouse. *Exp Eye Res*. 2014;125:226-235.
34. Hargrave A (2017). *Injury, Inflammation, and the Effect of the Metabolic Syndrome on the Mouse Cornea.* (Doctoral Dissertation, University of Houston, Houston, US).1-209.
35. Pal-Ghosh S, Tadvalkar G, Jurjus RA, Zieske JD, Stepp MA. BALB/c and C57BL6 mouse strains vary in their ability to heal corneal epithelial debridement wounds. *Exp Eye Res*. 2008;87(5):478-486.
36. Kumar V, Sharma A. Neutrophils: Cinderella of innate immune system. *Int Immunopharmacol*. 2010;10(11):1325-1334.
37. Mishalian I, Bayuh R, Eruslanov E, et al. Neutrophils recruit regulatory T-cells into tumors via secretion of CCL17 - A new mechanism of impaired antitumor immunity. *Int J Cancer*. 2014;135(5):1178-1186.
38. Lim K, Hyun YM, Lambert-Emo K, Capese T, Bae S, Miller R, Topham DJ, Kim M. Neutrophil trails guide influenza specific CD8+ T cells in the airways. *Science.* 2015;349(6252):1071-1081.
39. Adrover JM, Nicolás-Ávila JA, Hidalgo A. Aging: A Temporal Dimension for

Neutrophils. *Trends Immunol*. 2016;37(5):334-345.
40. von Vietinghoff S, Ley K. IL-17A Controls IL-17F Production and Maintains Blood Neutrophil Counts in Mice. *J Immunol*. 2009;183(2):865-873.
41. Hanlon SD (2012). *Neutrophil Interstitial Migration* (Doctoral Dissertation, University of Houston, Houston, US).1-215.
42. Yamashiro S, Kamohara H, Wang JM, Yang D, Gong WH, Yoshimura T. Phenotypic and functional change of cytokine-activated neutrophils: inflammatory neutrophils are heterogeneous and enhance adaptive immune responses. *J Leukoc Biol*. 2001;69(5):698-704.
43. Coxon A, Tang T, Mayadas TN. Cytokine-Activated Endothelial Cells Delay Neutrophil Apoptosis in Vitro and in Vivo. *J Exp Med*. 2002;190(7):923-934.
44. Petrescu MS, Larry CL, Bowden RA, et al. Neutrophil interactions with keratocytes during corneal epithelial wound healing: A role for CD18 integrins. *Investig Ophthalmol Vis Sci*. 2007;48(11):5023-5029.
45. Ley K, Laudanna C, Cybulsky MI, Nourshargh S. Getting to the site of inflammation: The leukocyte adhesion cascade updated. *Nat Rev Immunol*. 2007;7(9):678-689.
46. Sperandio M, Smith ML, Forlow SB, et al. P-selectin Glycoprotein Ligand-1 Mediates L-Selectin–dependent Leukocyte Rolling in Venules. *J Exp Med*. 2003;197(10):1355-1363.
47. Li Z, Burns AR, Han L, Rumbaut RE, Smith CW. IL-17 and VEGF are necessary for efficient corneal nerve regeneration. *Am J Pathol*. 2011;178(3):1106-1116.
48. Massberg S, Schaerli P, Knezevic-Maramica I, et al. Immunosurveillance by Hematopoietic Progenitor Cells Trafficking through Blood, Lymph, and Peripheral Tissues. *Cell*. 2007;131(5):994-1008.
49. Martinez-Bakker M, Helm B. The influence of biological rhythms on host-parasite interactions. *Trends Ecol Evol*. 2015;30(6):314-326.
50. Scheirmann C, Kunisaky Y, Frenette PS. Circadian control of the immune system. *Nat Rev Immunol*. 2013;13(3):190-198.
51. Scheiermann C, Kunisaki Y, Lucas D, et al. Adrenergic nerves govern circadian leukocyte recruitment to tissues. *Immunity*. 2012;37(2):290-301.
52. Wu H, Ghosh S, Perrard XD, et al. T-cell accumulation and regulated on activation, normal T cell expressed and secreted upregulation in adipose tissue in obesity. *Circulation*. 2007;115(8):1029-1038.
53. Jansson L, Carlsson P-O, Waldén TB, Phillipson M, Pettersson US. Female Mice are Protected against High-Fat Diet Induced Metabolic Syndrome and Increase the Regulatory T Cell Population in Adipose Tissue. *PLoS One*. 2012;7(9):1-10.
54. Kamezaki F, Sonoda S, Nakata S, et al. Association of seasonal variation in the prevalence of metabolic syndrome with insulin resistance. *Hypertens Res*. 2013;36(5):398-402.
55. Song F, Xue Y, Dong D, et al. Insulin Restores an Altered Corneal Epithelium Circadian Rhythm in Mice with Streptozotocin-induced Type 1 Diabetes. *Sci Rep*. 2016;6(32871):1-9.
56. Z. Li, Burns AR, Rumbaut R, Smith CW. Sex Differences in Corneal Epithelial Wound Healing in Mice. *Invest Ophthalmol.Vis Sci.* 2008;49(13):2403-2403.
57. Greenbaum AM, Link DC. Mechanisms of G-CSF-mediated hematopoietic stem and progenitor mobilization. *Leukemia*. 2011;25(2):211-217.
58. Wright, Douglas E.,Amy J. Wagers APG. Physiological Migration of Hematopoietic

Stem and Progenitor Cells. *Science* 2001;294(5548):1933-1936.
59. Ecoiffier T, Yuen D, Chen L. Differential distribution of blood and lymphatic vessels in the murine cornea. *Investig Ophthalmol Vis Sci*. 2010;51(5):2436-2440.
60. Weinberg DV, Egan KM SJ. Asymmetric distribution of arteriovenous crossings in the normal retina. *Ophthalmology*. 1993;100(1):31-36.
61. Scheiermann C, Kunisaki Y, Lucas D, et al. Adrenergic nerves govern circadian leukocyte recruitment to tissues. *Immunity*. 2012;37(2):290-301.
62. Hogg JC, Walker BA. Polymorphonuclear leucocyte traffic in lung inflammation. *Thorax*. 1995;50(8):819-820.
63. Gorbet M, Postnikoff C, Williams S. The noninflammatory phenotype of neutrophils from the closed-eye environment: A flow cytometry analysis of receptor expression. *Investig Ophthalmol Vis Sci*. 2015;56(8):4582-4591.
64. Rhee MK, Mah FS. Inflammation in Dry Eye Disease: How Do We Break the Cycle? *Ophthalmology*. 2017;124(11):S14-S19.
65. Pflugfelder SC, Stern M, Zhang S, Shojaei A. LFA-1/ICAM-1 Interaction as a Therapeutic Target in Dry Eye Disease. *J Ocul Pharmacol Ther*. 2016;33(1):5-12.
66. Wei Y, Asbell PA. The core mechanism of dry eye disease is inflammation. *Eye Contact Lens*. 2014;40(4):248-256.
67. Eckel-Mahan K, Sassone-Corsi P. Phenotyping Circadian Rhythms in Mice. *Curr Protoc Mouse Biol*. 2015;5(3):271-281.
68. Moore RY. The Suprachiasmatic Nucleus and the Circadian Timing System. *Elsevier Inc.* 2013; 119(1):2-22.
69. Potter, G. D., Skene, D. J., Arendt, J., Cade, J. E., Grant, P. J., & Hardie LJ. Circaidan Rhythm and Sleep Disruption: Causes, Metabolic Consequences, and Countermeasures. *Endocr Rev*. 2016;37(6):584-608.
70. Boivin DB, Boudreau P. Impacts of shift work on sleep and circadian rhythms. *Pathol Biol*. 2014;62(5):292-301.
71. Wang F, Yeung KL, Chan WC, et al. A meta-analysis on dose-response relationship between night shift work and the risk of breast cancer. *Ann Oncol*. 2013;24(11):2724-2732.
72. Anders Knuttsson HB. Gastrointestinal disorders among shift workers. *Scand J Work Environ Health*. 2010;36(2):85-95.
73. Hammer GP, Auvinen A, De Stavola BL, et al. Mortality from cancer and other causes in commercial airline crews: A joint analysis of cohorts from 10 countries. *Occup Environ Med*. 2014;71(5):313-322.
74. Méndez-Ferrer S, Lucas D, Battista M, Frenette PS. Haematopoietic stem cell release is regulated by circadian oscillations. *Nature*. 2008;452(7186):442-447.
75. Genewsky A, Heinz DE, Kaplick PM, Kilonzo K, Wotjak CT. A simplified microwave-based motion detector for home cage activity monitoring in mice. *J Biol Eng*. 2017;11(1):1-12.
76. Rieth S, Engel F, Bühner E, Uhlmann S, Wiedemann P, Foja C. Comparison of data from the rostock cornea module of the heidelberg retina tomograph, the oculus pentacam, and the endothelial cell microscope. *Cornea*. 2010;29(3):314-320.
77. Labbé A, Liang H, Martin C, Brignole-Baudouin F, Warnet JM, Baudouin C. Comparative anatomy of laboratory animal corneas with a new-generation high-resolution in vivo confocal microscope. *Curr Eye Res*. 2006;31(6):501-509.